UC San Diego
UC San Diego Previously Published Works

Title
A Reassessment of the Chronostratigraphy of Late Miocene C3–C4 Transitions

Permalink
https://escholarship.org/uc/item/3b5912rr

Journal
Paleoceanography and Paleoclimatology, 35(7)

ISSN
2572-4517

Authors
Tauxe, L
Feakins, SJ

Publication Date
2020-07-01

DOI
10.1029/2020pa003857

Peer reviewed

A re-assessment of the chronostratigraphy of late Miocene C₃-C₄ transitions

L. Tauxe[1] and S.J. Feakins[2]

[1]Scripps Institution of Oceanography, University of California San Diego, La Jolla, CA, 92093-0220
[2]Dept. Earth Sciences, University of Southern California, Los Angeles, CA, 90089

Key Points:

- A change from forest to grassland ecologies began in the late Miocene but chronologies of the published records are based on different time scales.
- Recalibration to a consistent time scale demonstrates the diachroneity of the ecological change in different places around the globe.
- New constraints link a major C_4 expansion in the late Miocene with evidence for carbon cycle perturbations.

Corresponding author: Lisa Tauxe, `ltauxe@ucsd.edu`

Abstract

Combining magnetostratigraphic and carbon isotopic data for the late Miocene can provide a temporal framework for an isotopic shift first documented in soil carbonate nodules of northern Pakistan. The shift has been interpreted as a change in vegetation from trees and shrubs (using the C_3 photosynthetic pathway) to grassland (using the C_4 pathway). The cause of the event has been hotly debated and its timing is close to a shift in carbon isotopes in the marine realm. Further understanding depends critically on timing.

Unfortunately, temporal calibration of the various records published over decades relied on different time scales. To address the lack of a consistent chronology, we have re-evaluated the constraints for the carbon isotopic shifts recorded from the Indian sub-continent. These show a diachronous transition ranging in age from about 7.8 Ma in Pakistan to as late at 6 Ma in Nepal. The record from IODP Expedition 355 Site U1457, drilled on the Indus fan shows that the transition in peninsular India began at about 7.2 Ma. Similar records from the African margin saw an earlier shift to C_4 dominance starting around 10 Ma and those from Australia and South America transitioned later, during the Pliocene. The diachroneity around the globe does not invalidate pCO_2 as a driver, but is consistent with it being one of several drivers of the global C_4 expansion.

Plain Language Summary

Grasslands expanded on the Indian sub-continent in the late Miocene. Precise chronological control is critical to compare the timing of the expansion between regions and to evaluate the possible causes (and consequences) of the ecological transformation. Here we take a new look at published records from Pakistan, India and Nepal and update the age models to a modern geomagnetic reversal timescale. We then compare these to new records from the marine sediments obtained during IODP Expedition 355 to the Indus Fan and others from the African margin. Based on microfossil appearance and paleomagnetic constraints, the timing of the transition to C_4 vegetation is found to be asynchronous across the globe, probably initiating in Africa after 10 Ma, then proceeding to Pakistan at around 7.8 Ma and reaching Nepal by ~6 Ma. Elsewhere in the world (Australia and Argentina) the transition happened several million years later. We also review recent model and proxy evidence to find the causes of the C_4 grassland expansion.

1 Introduction

The classic papers of Cerling et al. (1993) and Cerling et al. (1997) (based on earlier work by Quade et al. (1989)) introduced the hypothesis that an expansion of C_4 grasses in the late Miocene was linked to a global driver: a putative drop in pCO_2 in the atmosphere. However constraining pCO_2 in the ancient atmosphere is notoriously difficult (see, e.g., Cerling (1992)), and alkenone carbon isotopic records published by Pagani et al. (1999) shortly after that by Cerling et al. (1997) found no evidence for changes in pCO_2 in the late Miocene. Thus the CO_2-hypothesis as a driver for change in vegetation in the late Miocene fell out of favor, and other drivers including aridity, herbivory and fire were considered more likely (e.g., Osborne (2008)). However, a global pCO_2 change would not trigger a synchronous C_4 expansion as thresholds exist in other climatic variables including temperature, rainfall and fire as demonstrated for Africa by Higgins and Scheiter (2012).

Zhou et al. (2018) recently modeled the role of various climatic drivers (CO_2, temperature, water and light) in controlling the competitive advantage of C_3 versus C_4 vegetation globally using a fully coupled climate model under mid Miocene conditions run with three pCO_2 concentrations to bracket the range of estimates for the Oligocene to late Miocene (see Figure 1). Simulations run at 600 ppm pCO_2, suggested that water

61   limitation determined a few 'hot spots' where C_4 adaptations could emerge including in
62   northern Africa and central Asia and to a lesser extent western North America, south-
63   ern South America and Africa and western Australia (Figure 1a) and these could be lo-
64   cations were early C_4 evolution innovations occurred (Edwards et al., 2010). For pCO_2
65   of 400 ppm, the optimality of C_4 plants increased in these regions and was favored over
66   much larger regions, driven primarily by lower pCO_2 with feedbacks of increased light
67   as the canopy opened (Figure 1b). Under low pCO_2 (270 ppm) shown in Figure 1c, op-
68   timal conditions for C_4 dominance would have intensifed and expanded. However, this
69   scenario sees increases in C_4 coverage beyond that reported in late Miocene reconstruc-
70   tions (especially in places like East Asia and Australia) and thus may be a sign that such
71   low pCO_2 levels were not reached in the late Miocene. Testing the completeness of the
72   forcing assumptions in these simulations requires both a knowledge of CO_2 variations
73   and an accurate chronology for when vegetation changes occurred around the globe.
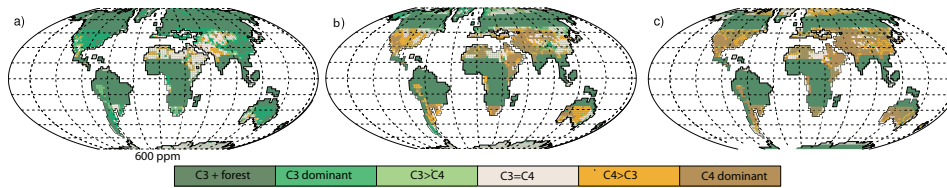

Figure 1.   Map of predictions of C_3 versus C_4 dominance under various pCO_2 scenarios: a)
600 ppm, b) 400 ppm and c) 270 ppm CO_2. [Figure modified from Zhou et al. (2018)].

74   Estimating pCO_2 in the past is a difficult problem (see for example commentary
75   by Beerling and Royer (2011)). Many proxies have been developed and some have data
76   in the late Miocene interval ($\delta^{11}B$; Sosdian et al. (2018), B/Ca; Tripati et al. (2009), alkenones;
77   Pagani et al. (1999), leaf stomata; Van der Burgh et al. (2009), ; diatom frustules; Mejia
78   et al. (2017), foraminiferal $\Delta^{13}C$; Holbourn et al. (2018) and paleosol carbonates (Cerling,
79   1992). These data were reported on different time scales and the details of precise dates
80   are frequently obscure (e.g., which time scale was used). For example, the leaf stomata
81   data of Van der Burgh et al. (2009) are poorly calibrated with respect to age and it is
82   difficult to tie them to the tight temporal framework required for inter-calibration. A
83   larger problem is that none of the pCO_2 proxies agree with each other (see compilation
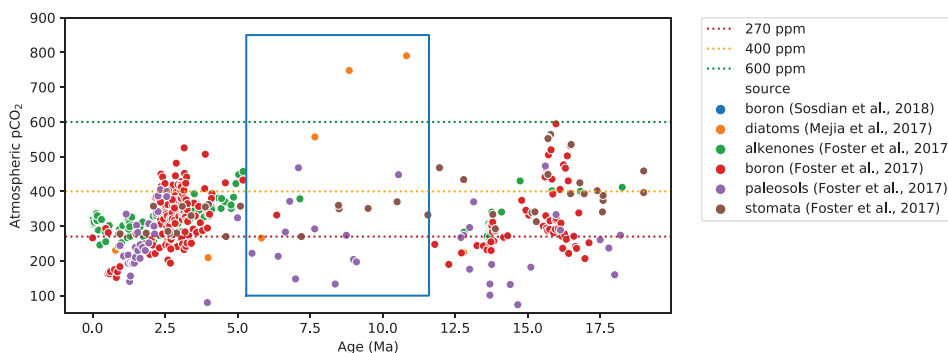84   of Foster et al. (2017) in Figure 2).

Figure 2. CO_2 proxy data synthesized in Foster et al. (2017), and updated with data from
Mejia et al. (2017), and Sosdian et al. (2018), colored by proxy type and data source. The box is
the late Miocene interval of interest in this paper.

The interval of interest here of the late Miocene (shown in the box in Figure 2) has a very sparse data set and little agreement among the various types of proxies. According to the compilation of Foster et al. (2017), there is no convincing evidence for a significant change in pCO$_2$ since the early Miocene except for the high values found in between 15 and 17 Ma and those from about 3 to 2.5 Ma which have been associated with the mid-Miocene Climatic Optimum and the Pliocene warm interval respectively. More recent records, such as the data from Δ^{13}C of organic matter within diatom frustules of Mejia et al. (2017) suggest high pCO$_2$ and a drop from a high of 800 ppm to 200 ppm with the peak at around 11 Ma and the drop beginning at around 8 Ma.

A recent data set from (Holbourn et al., 2018) based on foraminiferal Δ^{13}C records from planktic and benthic foramifera from ODP Site 1146 (shown in Figure 3) are the most detailed for the interval of interest here and can be placed on the time scale used here (Gradstein et al., 2012). These data provide no quantitative estimate of pCO$_2$, however. Nonetheless Δ^{13}C data are interpreted to indicate a drop in pCO$_2$ values between $\sim$7 and $\sim$7.5 Ma, possibly synchronous with part of the carbon isotopic shift in plant proxies discussed in this paper. Thus, these new pCO$_2$ proxies and the modeling efforts of (Zhou et al., 2018) reawaken a possibility of pCO$_2$ mediating the regional C$_4$ expansion in a diachronous progress as modification of the mechanism for a global synchronous transition envisioned by Cerling et al. (1993) and Cerling et al. (1997).

In this paper, we revisit the timing of the C$_4$ expansion around the globe by compiling published records and updating the magnetostratigraphic framework for their collective re-interpretation. This is an important step as the age of a single reversal in the time period of interest, for example the termination of Chron C4n, changed from $\sim$ 6.3 Ma in the time scale of LaBrecque et al. (1977) to $\sim$7.5 Ma in the current standard of Gradstein et al. (2012). In addition, we present a new record from IODP Site U1457 which has carbon isotopes from leaf waxes (Feakins et al., This volume), and reasonable chronostratigraphic constraints from biostratigraphy and magnetostratigraphy (Routledge et al., 2019), updated here. We also consider other recent records of leaf wax carbon isotopes recovered in DSDP and ODP cores taken around Africa (Feakins et al., 2013; Uno et al., 2016; Polissar et al., 2019) that have common biostratigraphic tie points.

Once the timing of the change in vegetation on the Indian sub-continent is secured, we can ask what combination of climate and CO$_2$ factors drove the C$_4$ expansion. We can also ask whether there is positive C$_4$ feedback on the carbon cycle. Commonalities of the timing of C$_4$ expansion and a shift in the δ^{13}C of marine carbonates (Feakins et al., This volume) have been noted. Grasslands can be quite efficient at sequestering CO$_2$ in soils (Fornara & Tilman, 2008; Spiesman et al., 2018; Yang et al., 2019) in comparison to the thin soil under the C$_3$ forests they replaced in the Indian sub-continent (although elsewhere replaced C$_3$ grasses (Feakins et al., 2013)). This positive feedback in turn could enhance global cooling (e.g., Retallack (2013); Retallack et al. (2018)).

2 Timing of the C$_3$-C$_4$ transition

2.1 The marine realm

In addition to the carbon isotope shift on land first detected by Quade et al. (1989) and expanded on by Cerling et al. (1993), there is also a marked carbon isotope transition recorded in deep sea sediments at about the same time. In fact, the story of the late Miocene shift in carbon isotopes began with a study by Keigwin of deep sea sediments (Keigwin, 1979). He documented a mysterious decrease of up to 0.8‰ in the $\delta^{13}C$ in benthic foraminifera in Deep Sea Drilling Project (DSDP) cores recovered at Site 158 in the Panama Basin (Easternmost Pacific) and Site 310 (Hess Rise) in the North Pacific (Figures 4a and 5 and Table 1). Keigwin inferred an age for the shift of $\sim$ 6.5 Ma based on correlation of the biostratigraphy (including the first occurence (FO) of *Cer-*
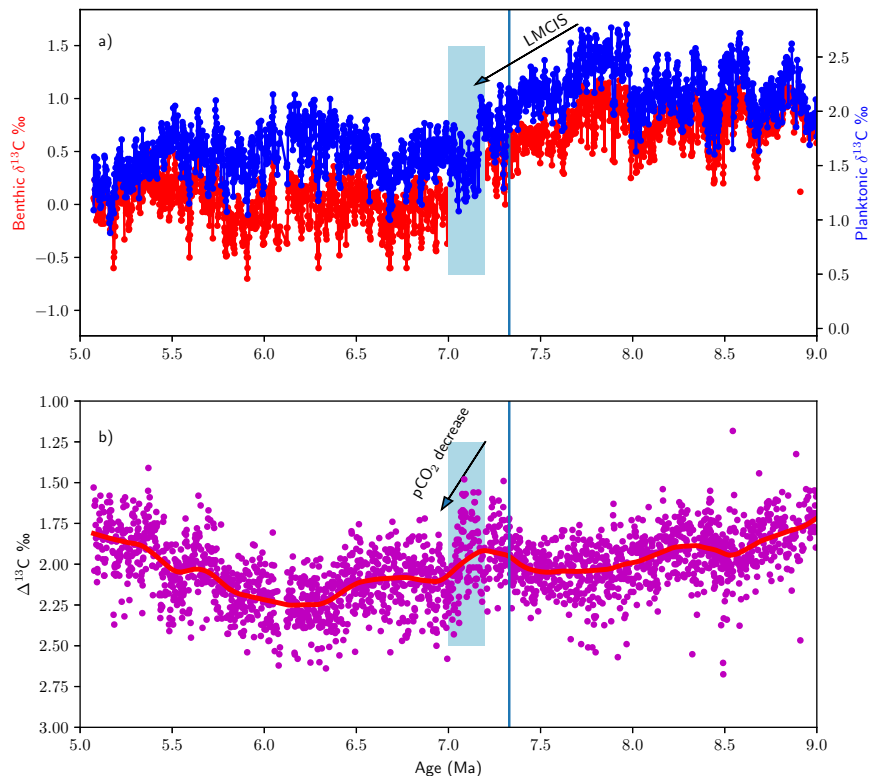
Figure 3. a) Benthic (red) and planktic (blue) $\delta^{13}C$ data of Holbourn et al. (2018) from ODP Site 1146. Blue vertical line is the FO of *Amaurolithus primus* at that site. The "Late Miocene carbon isotope shift" (LMCIS) from 8 Ma to 6.8 Ma is shown as in Holbourn et al. (2018). b) Difference between planktic and benthic $\delta^{13}C$ ($\Delta^{13}C$), plotted with lower values to the top. Higher values have been interpreted as resulting from lower atmospheric pCO₂ concentrations. The decrease in pCO₂ inferred between 7.2 and 7.1 Ma is as in Holbourn et al. (2018).

135   *atolithus primus* (now known as *Amaurolithus primus*), a diagnostic nannofossil. This
136   datum had been tied to the middle of "Epoch 6" (Theyer & Hammond, 1974) or in mod-
137   ern parlance Chron C3B, now estimated at 7.4 Ma in the GTS12 time scale of Gradstein
138   et al. (2012) (see also Raffi et al. (2006)). We note that Schneider (1995) tied this marker
139   to the middle of C3Br.2r so it is more likely to be 7.3 Ma, the age adopted here. Bender
140   and Keigwin (1979) suggested that the shift might reflect "either a global decrease in
141   upwelling rate or a different abyssal circulation pattern before the shift."

142   Shortly after the discovery by Keigwin, Vincent et al. (1980) found similar shifts
143   in the Indian Ocean at DSDP Site 238 (Figures 4a and 5), also closely associated with
144   the FO of *A. primus.* Vincent et al. (1980) echoed Keigwin in explaining the shift as re-
145   sulting from "changes in ocean circulation". The Vincent et al. study was immediately
146   followed by the study of Haq et al. (1980) who found the same shift occurring just af-
147   ter the FO of *Amaurolithus spp.* (i.e., *A. primus*?) in the world's oceans.
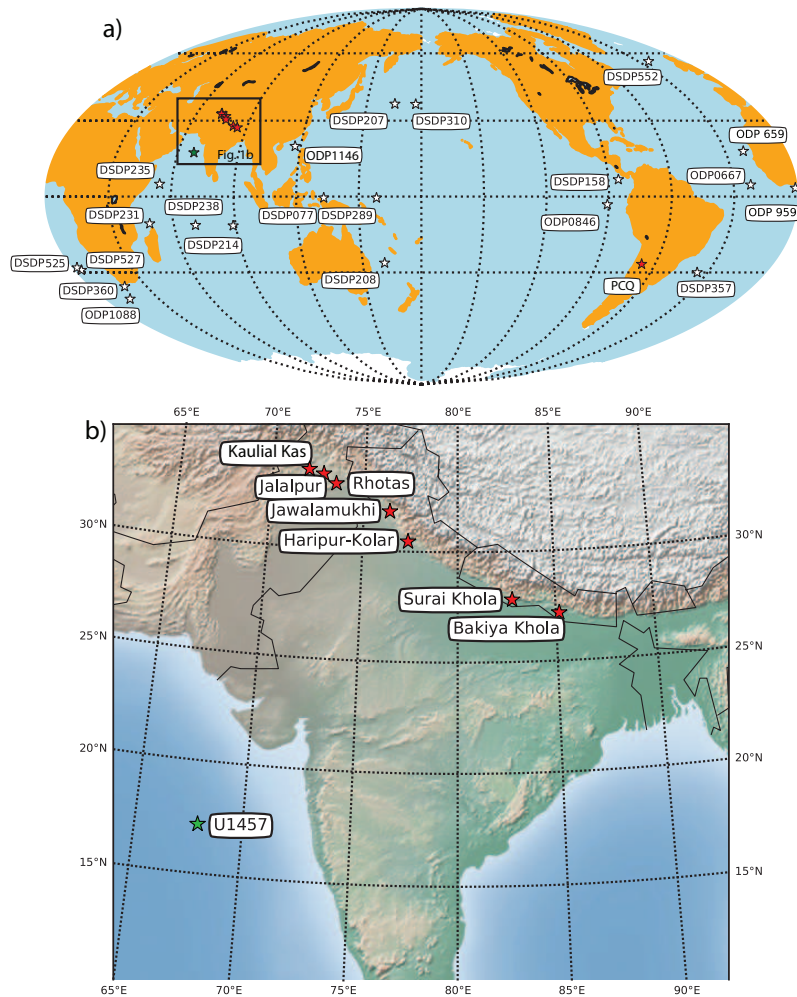
Figure 4. Map of locations of studies cited in this paper showing a) global compilation, b) Indian subcontinent and margins. See Table 1 for references.

¹⁴⁸ More recently, Cramer et al. (2009) compiled records from Deep Sea Drilling Project

¹⁴⁹ (DSDP) and Ocean Drilling Program (ODP) cores with benthic foraminiferal carbon iso-

¹⁵⁰ topic data (δ^{13}C) organized by ocean basin. In this way, water mass differences between

¹⁵¹ basins resulting from ocean circulation patterns are held separate, allowing for detection

¹⁵² of global carbon isotopic transitions rather than artifacts of the averaging of a varied num-

¹⁵³ ber of records with ocean basin bias. Because we are interested in the precise timing of

¹⁵⁴ the carbon isotope shifts relative to each other, we consider only those records that also

¹⁵⁵ have the FO of *Amaurolithus spp.* (see Figure 5 and Table 1). We plot the different records

¹⁵⁶ against stratigraphic depth relative to the FO of *Amaurolithus spp.* in Figure 5. There

¹⁵⁷ does appear to be a decrease in $\delta^{13}C$ associated with the FO of *Amaurolithus spp.* in

¹⁵⁸ many records, but some occur prior to the biostratigraphic datum (e.g., ODP1088) while

¹⁵⁹ others show no change at all (DSDP 552).

¹⁶⁰ ## 2.2 Records from the continents

¹⁶¹ Starting with Quade et al. (1989), the focus of Miocene carbon isotopes studies shifted

¹⁶² to the continents. They found a large (∼10‰) increase in δ^{13}C values in paleosol car-

¹⁶³ bonate of the Siwalik sequence of Pakistan which they interpreted as the signature of

Table 1. Locations of studies cited in the text. Rhotas is a composite of two sections (Dhabwala & Basawa Kas).

Site/Section	Lat.	Lon.	FO *A. spp.* (mbsf/*mcd*)	Ref.
DSDP077	-0.48	133.23	130	Keigwin and Corliss (1986), Woodruff et al. (1981), Woodruff and Savin (1989)
DSDP158	6.63	-85.24	150	Keigwin (1979)
DSDP207	36.96	165.43	94	Haq et al. (1980)
DSDP208	-26.11	161.22	180	Haq et al. (1980)
DSDP214	-11.34	88.72	128	Haq et al. (1980)
DSDP231	-11.89	48.25	384.1	Feakins et al. (2013), Fisher et al. (1974)
DSDP235	3.23	52.68	273	Uno et al. (2016), Party (1974)
DSDP238	-11.15	70.53	188	Haq et al. (1980)
DSDP289	-0.50	158.51	224	Woodruff et al. (1981)
DSDP310	36.85	176.90	68	Keigwin (1979)
DSDP357	-30.00	-35.56	24.135	Cramer et al. (2009)
DSDP360	-35.85	18.10	139.5	Wright et al. (1992)
DSDP525	-29.07	2.99	98.6	Shackleton et al. (1984)
DSDP527	-28.04	1.76	104.5	Shackleton et al. (1984)
DSDP552	56.04	-23.233	127	Cramer et al. (2009)
DSDP659	18	-21	180.24	Polissar et al. (2019). Ruddiman et al. (n.d.)
ODP0846	-3.09	-90.82	251	Diester-Haass et al. (2006)*
ODP0667	4.57	-21.91	107	Curry and Miller (1989)
DSDP959	3.5	-2.6	107.35	Polissar et al. (2019), Backman et al. (2012)
ODP1088	-41.14	13.56	71	Billups (2002), Hodell et al. (2002)
U1457	17.17	67.93	645	This study, Feakins et al.(this volume)
Kaulial Kas	333.34	72.70		Tauxe and Opdyke (1982) Quade et al. (1995)
Rhotas:				
Dhabwala Kas	32.95	73.58		Behrensmeyer et al. (2007) Opdyke et al. (1979)
Basawa Kas	32.95	73.579		Behrensmeyer et al. (2007)
Jalalpur	32.75	73.42		Quade and Cerling (1995) Johnson et al. (1982)
Jawalamukhi	31.8	76.39		Vögeli et al. (2017) Meigs et al. (1995)
Haripur Kolar	30.46	77.39		Vögeli et al. (2017) Sangode et al. (1996)
Surai Khola	27.82	82.79		Rösler et al. (1997); Neupane et al. (2019), Ojha et al. (2009); Quade et al. (1995)
Bakiya Khola	27.17	85.173		Quade et al. (1995) Harrison et al. (1993)
PCQ	-26.6	-66.9		Latorre et al. (1997) Butler et al. (1984)

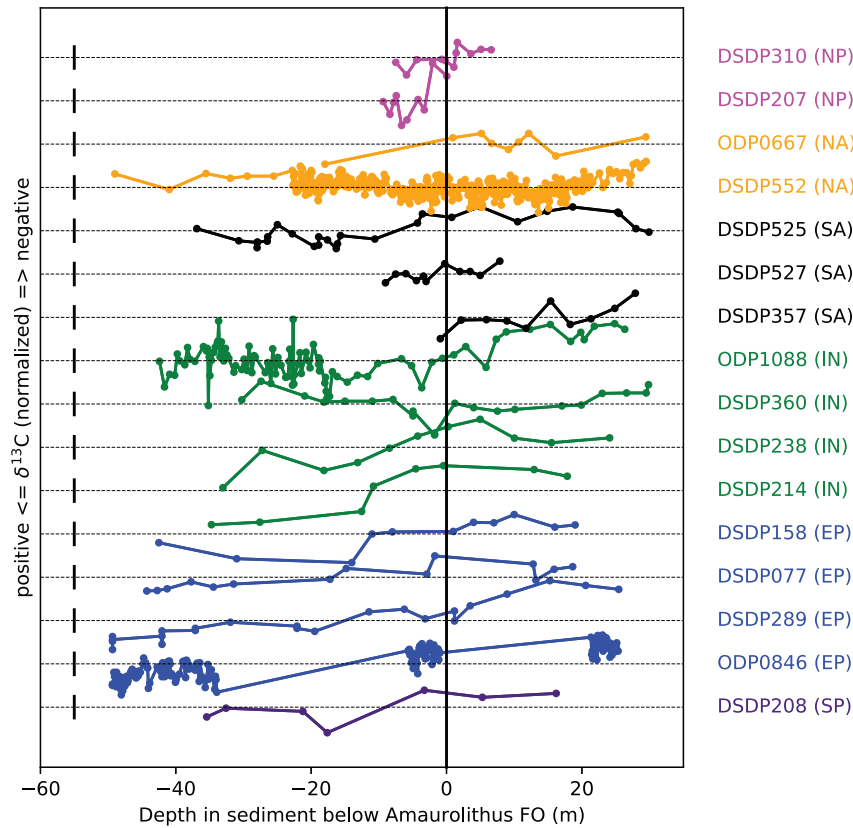**Figure 5.** a) Carbon isotopic shift in marine sediment cores (see Table 1 for locations and references). Values for δ^{13}C (normalized) are δ^{13}C - the mean value, plotted with more negative values up. Black bars to the left are $\pm 0.5‰$. X axis shows depth relative to the FO of *Amaurolithus spp.*, which occurs within Chron C3Br, now estimated to be 7.3 Ma (see text). Colors reflect regions where NP: North Pacific (magenta), NA: North Atlantic (orange), SA: South Atlantic (black), IN: Indian Ocean (green), EP: East Pacific (blue), SP: South Pacific (indigo). DSDP/ODP Site same as in Figure 4.

a change in vegetation from what is known as the "C$_3$ photosynthetic pathway" plants using the C$_3$ photosynthetic pathway to grasses using the C$_4$ pathway (see e.g., Tipple and Pagani (2007)). Quade et al. (1989) tentatively suggested that the shift could be related to an intensification of the Asian monsoon. Later, Cerling et al. (1993) reinterpreted the shift as resulting from a drop in atmospheric pCO$_2$ which would favor C$_4$ vegetation.

The Siwalik isotopic data were directly tied to magnetostratigraphic sections, constraining the shift to be within "Chron 6" which was renamed C3Ar and C3B. The geomagnetic reversal time scale (GRTS) used by Quade and Cerling (1995) was that of Berggren et al. (1985), hence their estimated age for the transition of between about 7.4 Ma and 6 Ma.

The approach of tying carbon isotopic data from continental sections to the GRTS has since been replicated elsewhere in Pakistan, India and Nepal as well as in Africa and South America. Latorre et al. (1997) and Singh et al. (2011) compiled data from continental sections, some of which were magnetostratigraphically calibrated. Their compilations suggested that the shift ranged in age from 4 Ma in North America to as early

as 8 Ma in East Africa, with the Asian data from the Siwaliks of India, Pakistan and Nepal ranging in age from 6 to 7.4 Ma. However, the calibration of the GRTS itself has evolved significantly over the nearly four decades of research on the topic. Moreover, the different carbon isotopic records have in some cases an ambiguous relationship to magnetostratigraphic calibration (e.g, the East African and North American data) making temporal inferences much more difficult.

What is of critical importance in assessing potential causes and effects of the C_3-C_4 transition is the relative timing of events on land (the expansion of C_4 grasses) compared to the marine records of carbon isotopes and to proxies for atmospheric pCO_2. These three different types of records have been dated using a variety of methods and the time scales have changed considerably over the years resulting in uncertainties of millions of years in the exact timing of the disparate records. In this paper we attempt to re-calibrate the different records in terms of a consistent time scale, which will enable us to assess the relative timing of the C_4 expansion, climatic drivers and carbon cycle responses. To do this, we first find those continental records that have a reasonable tie to magnetostratigraphic companion records and recalibrate them to a single time scale (here, the GTS12 of Gradstein et al. (2012)). In Section 3.1 we begin with a recalibration of the data from Pakistan, India and Nepal. In Section 3.2 we discuss the constraints from South America. Unfortunately, there are no results from North American Miocene with both soil carbonate isotopes and published magnetostratigraphic data and the magnetostratigraphies from Africa are similarly ambiguous in their relationship to the isotopic records. In Section 3.3, we turn to a new marine record of carbon isotopes from the Indus Fan (IODP Site U1457) that has both the biostratigraphic (including the FO of *Amaurolithus*) and magnetostratigraphic constraints. We then consider data from leaf waxes found by drilling on the African continental margin that also are tied the FO of *Amaurolithus* and the last occurrence of *Discoaster hamatus* (which has an age of ~10.5 Ma.) Finally we discuss the implications of our newly calibrated isotopic shifts compared to atmospheric pCO_2 proxies and consider possible feed-backs in the system.

3 Revisiting the timing of the C_3-C_4 transition in continental settings

3.1 Pakistan, India, Nepal

Quade et al. (1989) and Quade and Cerling (1995) reported carbon isotopic data from paleosol carbonate nodules from many sections from Pakistan in order to determine the age of the C_3-C_4 ecological transition: the Chinji-Nagri section of Johnson et al. (1985), the Kaulial Kas section of Tauxe and Opdyke (1982), the Mirpur section of Opdyke et al. (1979), the Jalalpur section of Johnson et al. (1982), the Pabbi Hills section of Opdyke et al. (1979) and Gabhir Kas or Johnson et al. (1982). These were all converted to ages using the GRTS of Berggren et al. (1985). A section studied initially by Quade et al. (1989) was resampled for paleomagnetic analysis in order to provide a tighter age constraint and the updated section was published by Behrensmeyer et al. (2007). Of the Pakistani sections, only two span the transition in a single (in some cases composite) section: the Rhotas (R) (composite) section of Behrensmeyer et al. (2007) (a combination of Dhabawal Kas and Basawa Kas sections with magnetostratigraphy from Opdyke et al. (1979) and Behrensmeyer et al. (2007)), and Jalalpur (JP) (Quade & Cerling, 1995) with magnetostratigraphy from Johnson et al. (1982). Kaulial Kas (KK) (Quade et al., 1995), with magnetostratigraphy from Tauxe and Opdyke (1982) has the onset of the transition and is also included in the present study.

Vögeli et al. (2017) compiled records from a variety of sections in NW India including the Jawalamukhti, Haripur Kolar, Jogindernagar, Kaming, Jammu Hills, the Parmandal-Utterbeni and Kangra sections. The magnetostratigraphy for Jogindernagar was based on unpublished data of Maithani and Burbank and the original data could not be located for the present study. The Kaming section has an excellent magnetostratigraphic con-
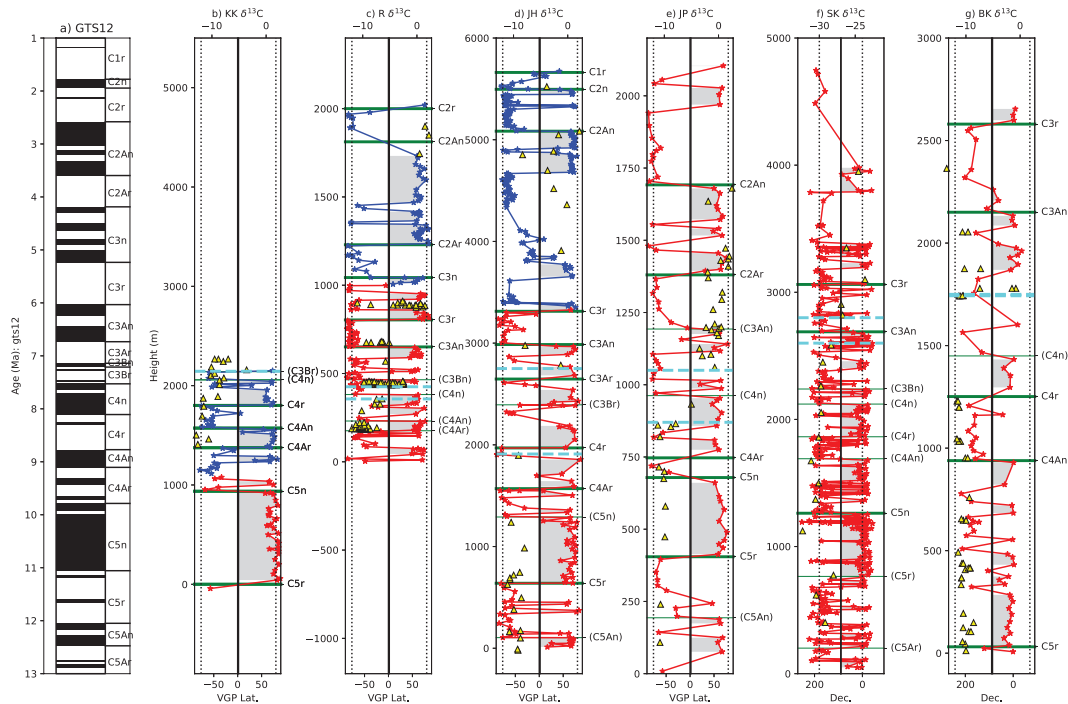
Figure 6. Magnetostratigraphic constraints for carbon isotopic data on the Indian subcontinent. a) GTS12 time scale of Gradstein et al. (2012) with the current Chron nomenclature. The magnetostratigraphy for each section is shown as virtual geomagnetic pole latitudes (VGP Lat.) or declination (Dec.) as a function of stratigraphic height in meters. Chrons are identified as in the original papers with heavy green horizontal lines, except for those in thin lines which are re-interpreted here (also placed in parenthesis). Isotopic data for each section are plotted as yellow triangles. The expected values for $\delta^{13}C$ (VPDB) for pure C_3 and C_4 biomass (-12 and 1.8‰ respectively from Quade (2014)) are plotted as vertical dotted lines in all sections except for SK which uses the bounds appropriate for plant wax *n*-alkanes (-30‰ is the upper limit of the C_3 plant waxes and -24‰ is the lower limit of C_4 for plant waxes). The stratigraphic bounds of the isotopic transitions are shown as cyan horizontal dashed lines. The sections are b) Kaulial Kas (KK), c) Rhotas composite (R), d) Jawalamukhi/Haripur (JH), e) Jalalpur (JP), f) Surai Khola (SK), g) Bakiya Khola (BK). See Table 1 for locations and references. More detailed views of these sections are shown in Figures S1-S7 in the Supplemental Information.

text (Chirouze et al., 2012) but the isotopes show no transition. The Jammu section only
has data through the Pliocene and the older data come from 50 miles away at Nurpur
with no published relationship to the magnetostratigraphy at Jammu. The data for Parmandal-
Utterbeni (magnetostratigraphy from Rao (1993)) only goes back through the Pliocene
and do not record the shift. The Kangra section (data in Sanyal et al. (2004)) come from
two different sections with no clear correlation to each other. Ghosh et al. (2017) pub-
lished isotopic data from several sections in India (Naladkhad, Ranital, Jabbarkhad and
Haripur Khol, or Haripur Kolar here). The magnetostratigraphic context for the Nal-
adkhad section is from Brozovic and Burbank (2000) and the isotopic sampling termi-
nated at about 1600 m, or C4An. The original magnetostratigraphic data from Rani-
tal are not in the reference cited (Sanyal et al., 2004) and the isotopic data show no change
from a C_3 dominated ecosystem throughout the section. They also report data from the
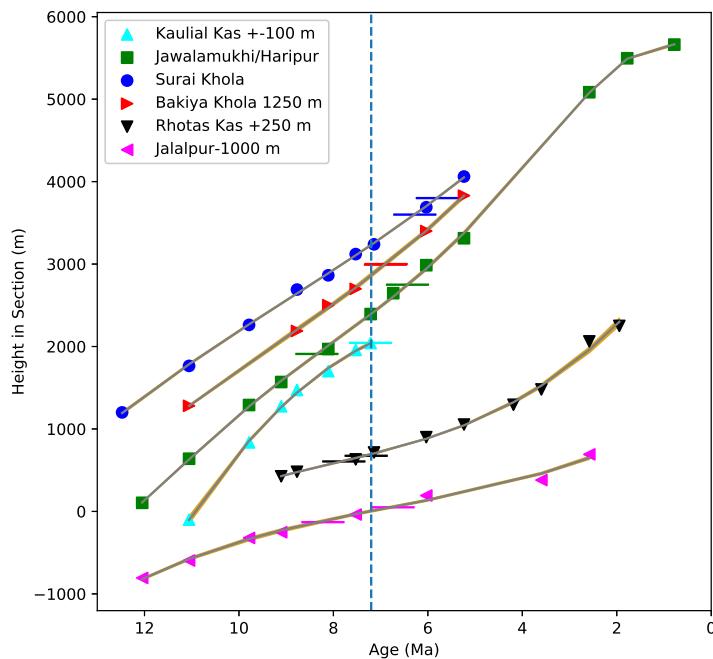upper part of Jabbarkhad (with magnetostratigraphy from Rao (1993)) and Haripur (with

Figure 7. Plots of stratigraphic heights of magnetostratigraphic tie points (Chron boundaries) for each section from Figure 6. Stratigraphic bounds on the isotopic shifts for each section (cyan horizontal lines in Figure 6) are shown as short horizontal bars for each section. A nominal age of 7.2 Ma is shown as a dashed vertical line, which passes through all the bounds except for those in the two Nepali sections (Bakiya and Surai Khola), whose bounds are younger. Reference heights for the different sections have been adjusted by various offsets to allow inter-section comparison. Kaulial Kas was shifted down by 100 m; Rhotas was shifted up by 250 meters; Bakiya Khola was shifted up by 1250 meters; Jalalpur was shifted down by 1000 meters. Polynomial fits are shown as yellow lines which are 1000 estimates using a Monte Carlo resampling scheme.

magnetostratigrahy from Sangode et al. (1996) and Sanyal et al. (2004)). The transition is not contained in any one of these sections. Therefore we focus on the Jawalamukhi and Haripur Kolar (JH) sections for the present study. These relied on magnetostratigraphic control from Meigs et al. (1995) and Sangode et al. (1996) respectively.

Isotopic data from Nepal were published by Quade et al. (1995) who investigated soil carbonates from the Surai Khola (SK) and Bakiya Khola (BK) sections in Nepal. More recently, Neupane et al. (2019) published new compound-specific data from leaf wax *n*-alkanes for Surai Khola. The Surai Khola data from Quade et al. (1995) and Neupane et al. (2019) have magnetostratigraphic constraints from Ojha et al. (2009) and Rösler et al. (1997) respectively and the Bakiya Khola isotopic data from Quade et al. (1995) have magnetostratigraphic data from Harrison et al. (1993). Quade et al. (1995) also presented data from Muksar Khola and Neupane et al. (2019) presented data from the Karnali River, but these sections do not show a shift in the carbon isotopes and in the case of Muksar Khola, they were not derived from pedogenic carbonate, the focus of the current study. Quade et al. (1995) also showed data from the Katari Khola section, but these

were only plotted versus stratigraphic height and we were unable to locate the original magnetostratigraphic data.

Most of the studies concerned with the C_3-C_4 transition in Asia plotted the isotopic data in terms of age and the exact relationship to the supporting magnetostratigraphic age control can be obscure. Therefore in order to recalibrate the age for the isotopic data using a consistent time scale, we digitized the magnetostratigraphic and isotopic data, converting both to a common stratigraphic height scale in order to obtain age-height relationships using the GTS12 time scale of Gradstein et al. (2012). C_3 plants have a range of carbon isotopic values from -38 to -18 ‰ (mean -26.7 ± 2.3‰) and C_4 plants have values of -16 to -9 ‰ (mean -12.5 $\pm$ 1.1 ‰; Cerling et al. (1997)) with corresponding boundaries in plant waxes (more depleted) and soil carbonates (more enriched). These can be used to place bounds on the stratigraphic position of the change in isotopic values, with the caveat that dry, open C_3 woodland can be indistinguishable from C_3 forest with some C_4 understory, thus there is always ambiguity in the interpretation of the first appearance of C_4 as appreciated in the discussion by Fox and Koch (2003), but often missed in presentations of C_4 %. Here the case is simplified as we are not looking to detect first appearance of C_4 or low proportions of C_4 in ecosystems, but rather focus on the shift to C_4 dominance and thus seek large positive isotope shifts that are unambiguous.

Our reconstructed magnetostratigraphic and isotopic data are shown in Figure 6. Using the information in the figure, bounds on the stratigraphic position of the isotopic shifts from C_3 dominated ecosystems to those dominated by C_4 vegetation can be converted to ages from GTS12 in a consistent manner.

The logic for calculation of an age model for magnetostratigraphic sections relies on several key assumptions:

1. We must assume that all magnetic directions (from which we determine polarity) are reliable.
2. In order to correlate a given section to the polarity time scale we must assume a quasi-linear or slowly varying sedimentation rate.
3. Sections must be sampled at a sufficient density to insure that all (or at least most) of the polarity intervals are represented.
4. To transfer ages from the magnetostratigraphic correlations to the isotopic data, the isotopic sampling must be done in close coordination with the magnetostratigraphic sampling, so that the stratigraphic section heights are the same.

In Kaulial Kas, the magnetic stratigraphy is densely sampled. Multiple samples per site allowed rejection of highly scattered (random) directions and the age model is fairly robust. The isotopic sampling was done on the same section as the magnetostratigraphy. Therefore all four conditions are met.

At Rhotas, the magnetic stratigraphy was sampled at sufficient density and was based on a reasonable laboratory protocol (step wise thermal demagnetization of multiple specimens per site) to insure that polarity identifications are robust. The isotopic sampling was done along side the magnetic stratigraphy so there is no ambiguity about the relationship of the two data sets.

In the NW Indian composite, the magnetic stratigraphy in the lower section (Jawalamukhi of Meigs et al. (1995)) is based on an undersampled section and the lab procedures followed the early protocol whereby extremely scattered within site directions were used, leading to the possibility of incorrect polarity assignments. The upper section at Haripur (Sangode et al., 1996) used a more sophisticated approach and reported within site statistics. While the lower part of the section had poor within site reproducibility in general, the upper part (relied upon here for the age model) can be considered "re-

liable". The isotopes of Vögeli et al. (2017) were sampled much later than the magnetostratigraphic sample and plotted against age. We combined the magnetostratigraphic data with the isotopic data by using the age model of Vögeli et al. (2017) to convert their ages back to stratigraphic height. Then, by pairing the inferred heights with the heights from the magnetostratigraphic studies, we attempted to recalibrate the ages for isotopic data. However, there is an added uncertainty in this process and condition 4 above was not met.

In the Jalalpur section, the original magnetostratigraphy of Johnson et al. (1982) was severely undersampled so condition 3 above was not met. Also, a very high degree of scatter ($k > 10$) was allowed and many sites that were based on random directions were deemed acceptable so condition 1 was not met. However, the isotopes were taken in coordination with the magnetic sampling sites so condition 4 was met.

There are several different data sets from Surai Khola. The most recent is the isotopic data set of Neupane et al. (2019). This was tied to the magnetostratigraphy of (Rösler et al., 1997) (which itself was updated from (Appel et al., 1991)). The section was densely sampled, but only one specimen per horizon (site) was measured so there are no within site statistics on which to assess condition 1. In the Kaulial section it was found that some 40% of sites had random within site directions and could be eliminated by using within site statistics, but that is not possible in the SK section of Rösler et al. (1997). However, stratigraphic height information relating the isotopic data to the SK section was made available by the authors of Neupane et al. (2019), so condition 4 was met.

At Bakiya Khola, the magnetostratigraphy was apparently based on single specimens per site so condition 1 was not met. Furthermore, the section is undersampled so condition 3 was also not met. However, the isotopic samples were taken in coordination with the magnetic sampling so condition 4 was met.

We plot stratigraphic height against the ages inferred from the correlation to GTS12 in Figure 7. Given the above mentioned caveats, we estimate sediment accumulation rates for each section by calculating a 3rd (or in the case of the NW Indian composite a 5th) order polynomial. To estimate the uncertainties for each curve we adopt a Monte Carlo resampling scheme whereby the depths of the tie points are drawn from uniform distributions between the upper and lower bounds for each calculate a new curve for each resampled set of tie points, repeating the process 1000 times. We plot each of the Monte Carlo curves in yellow on the figure. The stratigraphic bounds for the isotopic shift from each section are shown as horizontal lines.

An alternative approach to calculating an age model for these sections would be to assume all four of the conditions above are met and interpolate between magnetostratigraphic tie points using a straight-line calculated between the bounds. This assumes that sediment accumulation is essentially linear between each bounding tie point and can result in abrupt changes in rate between adjacent segments. We recalculated all ages using this approach and found that the difference between the smoothly varying approach (polynomial assumption) and the piece-wise linear approach was $\pm \sim 100,000$ years and much better than that near the interval of interest here (a few 10s of thousands of years). Given the additional uncertainties and assumptions associated with the second approach, We adopt the first, smoothly varying, approach in the following.

The first question we wish to address is whether there is a single age or age range for the isotopic transition that is consistent with all of the available data from the Indian sub-continent. We replot the data from Figures 6 and 7 as isotopes versus inferred age in Figure 8. In Figure 8b we plot the data from India and Pakistani sections (Kaulial Kas, Rhotas, Jawalamukhti/Haripur and Jalalpur) against the revised ages. The transition began perhaps as early as C4n ($\sim$7.8 Ma) as suggested by a single point in the Jalapur section, but certainly by C3Bn ($\sim$7.2 Ma) in the Kaulial and Rhotas sections.

In Figure 8c we plot the data from Nepal (Surai and Bakiya Khola). The transition recorded in Nepal started later than in Pakistan and India, perhaps as young as 6 Ma as recorded in Surai Khola. This diachroneity within a single subcontinent could argue against pCO_2 as the sole or even dominant driver of the process, although tipping points may differ across climatic regimes (Higgins & Scheiter, 2012). For example, the western side of the subcontinent (Pakistan) is considerably drier and thus may pass climatic thresholds that promote C_4 grasslands to replace forests earlier than the eastern side (Nepal). This observation is also supported by the modeling efforts of (Zhou et al., 2018) (Figure 1) which show considerable regional variability within a constant atmospheric pCO_2 regime.
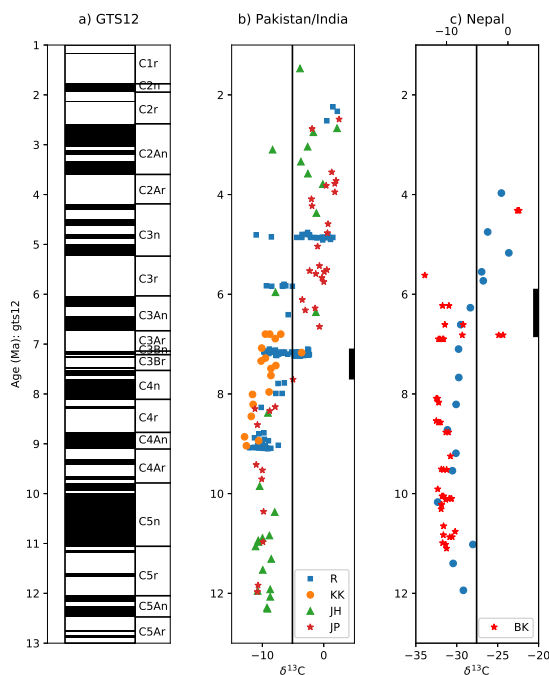
Figure 8. Isotopic data from Figure 6 plotted against age from Figure 7. Section abbreviations same as in Figure 6. See Table 1 for references. a) Time scale of (Gradstein et al., 2012). b) data from Pakistan and India. c) data from Nepal. Surai Khola has the latest onset of all sections. Black bars on side of b-c) are range for onset of C_4 dominated ecosystems in each region.

3.2 Other continental sections

To place the data from the Indian subcontinent into a global context, we look first to other records with good magnetostratigraphic control. While there are studies from Chinese Loess Plateau (e.g., Dong et al. (2018)), these have not yet been placed in a magnetostratigraphic context. In any case, the study focused on the Mid-Miocene Climatic Optimum (much earlier than the focus of this paper) and demonstrated that there may have been a slight increase in the percentage of C_4 plants at around 15 Ma as two data points are close to a 50% C_4 fraction.

Ségalen et al. (2007) cited data from Africa but those do not show the clear transition to C$_4$ values and the data are not clearly tied to the available magnetostratigraphic sections (which are in an unpublished master's thesis and do not stand up to scrutiny). Uno et al. (2011) published isotopic data from mammal teeth but the magnetostratigraphic data (as opposed to the interpretations) were apparently also never published. Similarly, Morgan et al. (1994) present data from mammal teeth from the Tugen Hills section (near the sections studied by Tauxe et al. (1985), but include no information about the relationship between their fossil localities and any magnetostratigraphic constraints.

North America appears to have no magnetostragraphically calibrated isotopic data either. However, Tipple and Pagani (2010) published isotopic data from DSDP Site 94 from the Gulf of Mexico. Unfortunately, the latter section lacks the FO of *A. primus* with which to tie the record to the present study. Moreover, it has only weak support for the onset of C$_4$ vegetation in the Miocene. Similarly, Chen et al. (2015) sampled sections in Montana relying on an age of 10.42 Ma for an ash bed reported by (Retallack, 2007) who in turn cited an unpublished field guide. The isotopes (which show a dominance of C$_3$ grasses throughout the section) are thought to range from $\sim$ 9 to $\sim$ 10.4 Ma. Finally, Fox and Koch (2003) published a set of soil carbonate isotopic data calibrated with the North American Land Mammal Ages. This data set suggests that by the Pliocene, the vegetation in western North America was dominated by C$_4$ vegetation.

The picture in South America, is much better constrained than for North America. Latorre et al. (1997) published isotopic data from soil carbonates from the Puerta de Corral Quemado (PCQ) section in Argentina which has excellent magnetostratigraphy control from Butler et al. (1984), which we show in Figure S8. The increasing abundance of C$_4$ plants is suggested by δ^{13}C values higher than -7.5 ‰ and the transition is well constrained to be younger than 4 Ma. This result agrees with other sections from Argentina that unfortunately lack magnetostratigraphic constraints (Kleinert & Strecker, 2001). The results from Argentina are similar to those of Andrae et al. (2018) who found a Pliocene onset for the C$_3$-C$_4$ transition as recorded in leaf wax data found in samples from ODP Site 763A off NW Australia. Therefore the C$_3$-C$_4$ transition in terrestrial sequences cannot be globally synchronous, in agreement with predictions by the modeling efforts of, for example, Zhou et al. (2018) (see Figure 1).

3.3 U1457: A Rosetta stone for carbon isotopes

Returning to the paleoceanographic carbon isotopic shift first noted by Keigwin (1979), the question arises as to how the transition in the Indian subcontinent relates to the paleoceanographically observed carbon shift. Until now, deep sea records of the carbon shift have been tied to the first occurence (FO) of *Amaurolithus spp.* The age of *Amaurolithus spp.* in GTS12 is stated to be 7.4 Ma. However, it was found in two Ocean Drilling Program (ODP) holes: 844B and 710B. The FO in 844B was found at 844B-5H-5; 29 cm which, according to Schneider (1995), is in the middle of C3Br.2r or about 7.3 Ma using the timescale of Gradstein et al. (2012). It was also found in 710B-7H-5,30/7H-4, 130 or 60.5 mbsf, an interval between C3Ar (y) and C4n (y). Assuming a linear sedimentation rate gives an approximate age for this datum of about 7.35 Ma. We adopt the former age of 7.3 Ma here as it is better constrained. What is required to tie the continental records to the marine records is a core in which the isotopic shift and the FO of *Amaurolithus spp.* both occur in a magnetostratigraphic context. IODP Site U1457 provides such an opportunity.

The nannofossil, foraminiferal, strontium isotope and paleomagnetic age constraints for Site U1457 were recently published by Routledge et al. (2019). Here we use their biostratigraphy and a revised interpretation of a few of the paleomagnetic age constraints (see Table 2 and Figure 9). The lithology of Site U1457 is shown in Figure 9. Routledge et al. (2019) defined six lithologic units at Site U1457 and used the age model shown in

Datum	Type	Event	Age (Ma)	Max. (m)	Min. (m)	Midpoint (m)
24	CN	T Sphenolithus spp.	3.540	517.45	513.09	515.27
26	CN	B Discoaster tamalis	4.130	539.15	539.65	539.40
28	CN	T Discoaster quinqueramus	5.590	539.65	539.15	539.40
29	PF	T Globoquadrina dehiscens	5.920	526.64	513.09	519.87
30	CN	T Nicklithus amplificus	5.940	610.36	610.05	610.21
32	MR	C3Ar	6.733	624.23	625.42	624.83
33	PF	B Pulleniatina primalis	6.600	615.50	621.36	618.43
35	CN	B Nicklithus amplificus	6.910	628.34	629.53	628.94
36	MR	C3Br.2r	7.285	643.04	644.16	643.60
38	CN	B Amaurolithus spp.	7.300	645.05	644.76	644.91
39	MR	C3Br.2n	7.454	662.92	664.92	663.92
41	MR	C4n.1r	7.642	674.47	675.62	675.05
42	CN	B Discoaster quinqueramus	8.120	832.85	845.62	839.24
43	CN	T Minylitha convallis	8.680	845.62	832.85	839.24
44	CN	T Discoaster bollii	9.210	856.50	845.62	851.06
45	CN	T Catinaster coalitus	9.690	864.64	856.50	860.57
46	MR	C5n	9.790	864.18	866.20	865.19
47	PF	B Neogloboquadrina acostaensis	9.830	885.02	894.30	889.66
48	CN	B Discoaster bellus	10.400	1001.08	1005.11	1003.10
49	CN	B Catinaster coalitus	10.890	1001.08	1005.11	1003.10
50	CN	Absence of Fasciculithus spp.	62.130	1068.63	1067.35	1067.99

Table 2. Age model revised from Routledge et al. (2019). B: bottom (or first occurrence), T: top (or last occurrence). Ages are as in Gradstein et al. (2012) except for *Amaurolithus spp.* (see text). All depths are in composite meters depth (CCSF) as in Routledge et al. (2019).

Figure 9b. Based the fact that Unit 4 contains several subunits with more or less carbonate or turbiditic sandstones (which substantially change the sediment accumulation rates), we now further subdivide Unit 4 into three packages (4a-c, see Figure 9c). The upper package (Unit 4a) is dominated by sandy layers, the middle package (Unit 4b) is dominated by carbonates and clays and the lower unit (Unit 4c) has a higher sand content as in Unit 4a. There are pronounced changes in sediment accumulation rates with inflection points at the unit boundaries. We have modified the age model from Routledge et al. (2019) to take into account the lithological changes and the resulting revised tie points are listed in Table 2 and on Figure 9c.

The sediment accumulation rate for Unit 4c was estimated by a linear fit to the two bounding tie points (28 and 30 in Table 2) as there are no additional internal controls. For Unit 4b, we used a 3rd order polynomial as with the Indian subcontinent analysis, with the Monte Carlo estimates shown in yellow. The higher sediment accumulation rate in the lower part of the unit is caused by the higher proportion of sandy layers). Unit 4a is dominated by turbidites and we again simply use a linear fit between the two bounding tie points (41 and 41). Unit 3 is clay/claystone and the age model is based on a linear fit between tie points 42 and 46. Unit 2 is a mass transport deposit.

Using the age model shown in Figure 9c, we plot the magnetostratigraphic and isotopic data for Unit 4b in Figure 10. The C_3-C_4 transition occurs just above the FO of *Amaurolithus spp* and within a normal interval interpreted here as C3Br.2n or at about 7.2 Ma. This is within the age interval for the transition in India and Pakistan estimated in Figure 8.
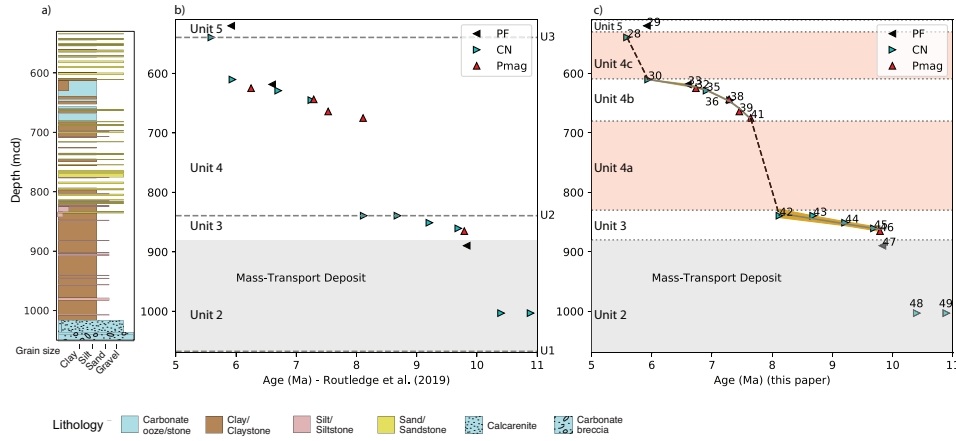
Figure 9. a) Lithostratigraphy for U1457 modified from Pandey et al. (2016) in meters composite depth (CCSF). b) Age model from Routledge et al. (2019). c) Revised age model for this study (see Table 2). PF: planktonic foraminifera, CN: calcareous nannofossils, Pmag: paleomagnetic Chron identifications.
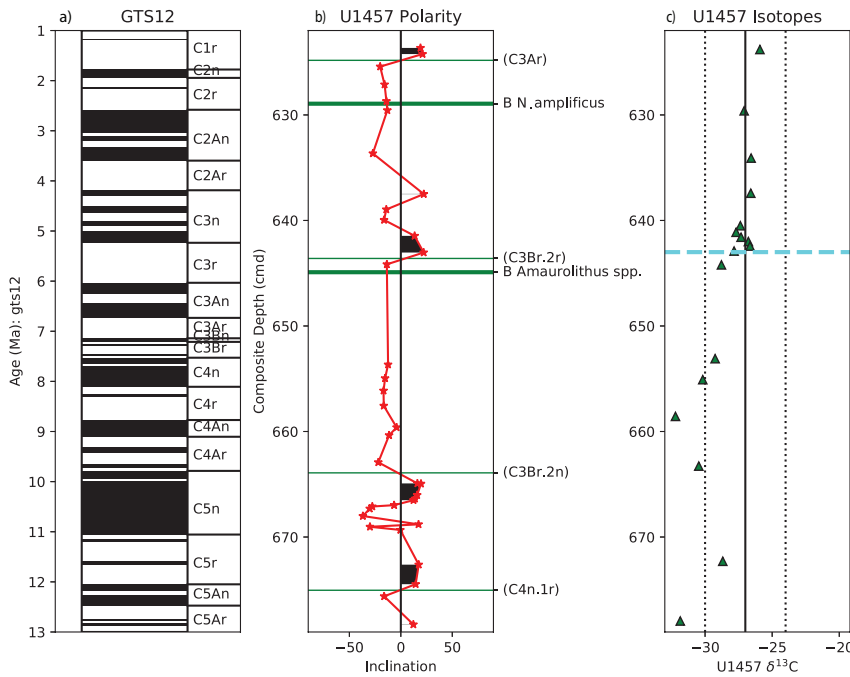

Figure 10. a) Geomagnetic reversal time scale of Gradstein et al. (2012). b) Magnetostratigraphic data for U1457 (Indus Fan) are from Routledge et al. (2019) as re-interpreted in Table 2. The Chron boundary picks minimize changes in sedimentation rate between hiatuses and minimize the discrepancy between the nannofossil identifications. Some Chron boundary picks and were adjusted slightly from the original publication (shown in parentheses). c) Isotopic data are from Feakins et al. (This volume). Magnetostratigraphic and isotopic data are plotted on the composite depth scale. Bounds for upper limit of C_3 and lower limit of C_4 (vertical dotted lines). Horizontal cyan dashed line is the transition between C_3 and C_4 vegetation.

The carbon isotopes were measured on leaf waxes whose inputs to the hemipelagic units are interpreted as being wind-transported based on a lack of associated lignin (both are present in the fluvially-export carried in turbidic units Feakins et al. (This volume). The wind-blown waxes are thought to derive from peninsular India based on the proximity of the continent, the dominant easterly winds in October-to-January and modern evidence from coretops across the Arabian Sea (Dahl et al., 2005).
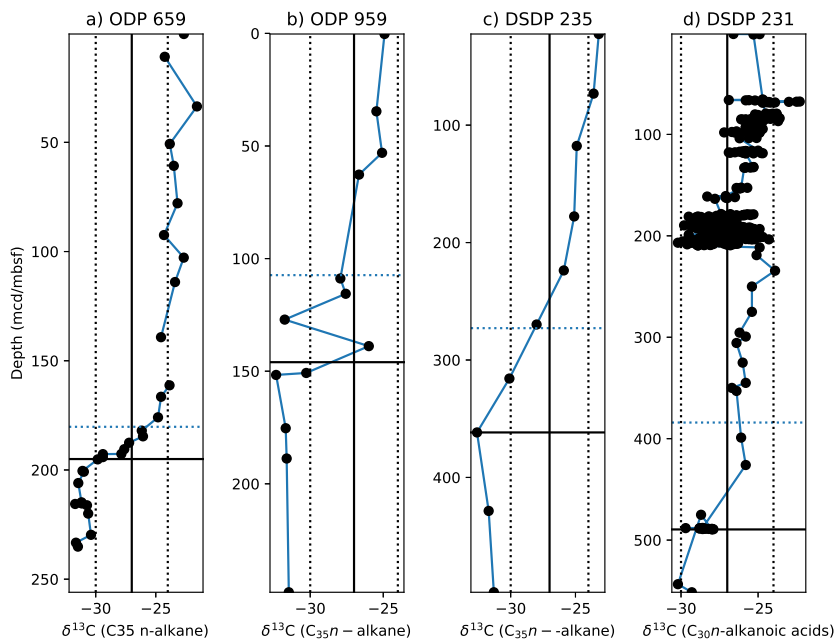
Figure 11. Leaf wax δ^{13}C C$_{35}$ *n*-alkane (a-c) and d) C$_{30}$ *n*-alkanoic acid data from deep sea cores around Africa (see Table 1 and Figure 4). Dotted horizontal lines are the first occurrences of *Amaurolithus spp.* in each core. Solid lines are the last occurrences of *Discoaster hamatus* with an age of 10.5 Ma. a) ODP Site 659; data from Polissar et al. (2019). b) ODP Site 959; data from Polissar et al. (2019). c) DSDP Site 235; data from Uno et al. (2016). d) DSDP Site 231 from Feakins et al. (2013).

3.4 Africa

As noted earlier, data from continental sections in Africa are insufficient to constrain the C$_3$-C$_4$ transition. However, analysis of leaf waxes found in DSDP and ODP cores, in connection with the FO of *Amaurolithus spp* can provide some clues. We plot the data from leaf wax δ^{13}C C$_{35}$ *n*-alkanes from Uno et al. (2016) and Polissar et al. (2019) and δ^{13}C C$_{30}$ *n*-alkanoic acids from Feakins et al. (2013) in Figure 11 against depth. We also show the FO of *Amaurolithus spp* and the last occurrences (LO) of *Discoaster hamatus* with an age estimated at ~10.5 Ma (Gradstein et al., 2012). These data suggest that the change in vegetation from C$_3$ dominated ecosystems to those dominated by C$_4$ occurred between these two tie points, sometime after about 10 Ma as suggested by (Polissar et al., 2019). These are the earliest ages for the transition that we know of and are consistent with the model of (Zhou et al., 2018) (Figure 1) whereby eastern Africa is one of the first places predicted to favor C$_4$ vegetation.

4 Discussion

From the re-analysis of age constraints for isotopic data from marine and continental sections it appears that there was at least a regional shift in carbon isotopes in Africa beginning sometime after 10 Ma, but well before 8 Ma. Data from U1437 (Indus Fan) suggests an age of 7.2 Ma for peninsular India. In Northern Pakistan and NW India, the change began perhaps as early as 7.8 Ma (based on a single data point from Jalalpur) but certainly by about 7.2 Ma. Vegetation in Nepal shifted somewhat later, after 7 Ma, and data from Argentina and Australia indicate that the shift occurred in the Pliocene. Moreover, using the first occurrence of *Amaurolithus spp.* as a temporal marker, we can tie the record from U1457 to other marine records of carbon isotopes (for example, the leaf wax data of Uno et al. (2016) recovered at DSDP Site 235, of Feakins et al. (2013) at DSDP Site 231 and of Polissar et al. (2019) from ODP Sites 659 and 959) which show that the shift in carbon isotopes in Africa likely pre-dated the marine carbon isotope shift first recognized by Keigwin (1979) and was well before that recorded elsewhere. The question remains as to how these ecological changes fit with possible drivers, a topic to which we now turn.

Raymo and Ruddiman (1992) made the case that uplift of the Himalayan region and the Tibetan Plateau could have resulted in higher chemical weathering which in turn could have resulted in a drawdown of atmospheric CO_2. While the Himalayas are broadly believed to have been at high elevations much earlier than the shifts examined here, there are some signs of uplift in the late Miocene. Harrison and Yin (2004) suggested a major phase of uplift at around 9 Ma and Molnar et al. (1993) interpret the onset of normal faulting in Tibet at around 8 Ma as evidence of an uplift of the plateau. Interestingly, Tremblay et al. (2015) call for decreased erosion in southern Tibet caused by enhanced uplift at about 10 Ma, an effect opposite to the mechanism envisioned by Raymo and Ruddiman.

Changes in the carbon budget may also arise from often overlooked adjustments in the global organic carbon cycle and the case has been made that enhanced organic carbon burial in the Bengal Fan could outweigh any changes in silicate weathering (Derry & France-Lanord, 1996). It is also possible that the rise of C_4 grasslands led to a change in the carbon cycle with attendant climate feedbacks. A large-scale change in ecology could shift the balance of carbon storage as forests have generally thin soils whereas grasslands can build deep soils. Limited evidence from experimental farms in Minnesota, (Fornara & Tilman, 2008) estimated that C_4 vegetation pulls down 193% more carbon into the soil than C_3 vegetation. More recently, Spiesman et al. (2018) found that, depending on the quality of the soil, a higher proportion of C_4 grasses relative to C_3 grasses can indeed enhance carbon storage; they attribute this to the higher efficiencies in nitrogen and water usage by the C_4 photosynthetic pathway.

Even if only part of the Indian sub-continent were covered by C_4 grasses, and the resulting paleosols buried (as they were in the Siwaliks), this could provide a positive feedback as lower pCO_2 would in turn favor the C_4 grasses. Whatever the mechanism, the current array of pCO_2 reconstructions do leave open the possibility of a late Miocene pCO_2 drop that would have enhanced the viability of C_4 plants.

4.1 Conclusions

In this study we reconsider the timing of the shift to C_4 dominance in ecosystems around the world. We have been able to realign records where the following conditions are met:

1. Marine data include the first appearance of *Amaurolithus spp.*
2. Magnetostratigraphic records are provided including the depth in section of the chronostratigraphic markers in order for alignment as chronostratigraphy evolves.

We emphasize that making the age model data available alongside new carbon isotope records is particularly valuable for ensuring that updated comparisons can be made as chronologies evolve. Some regions that are missing from the present comparison are on land in North America where magnetostratigraphic age control would greatly improve interpretations.

Leaf wax data from offshore of Africa (Feakins et al., 2013; Uno et al., 2016; Polissar et al., 2019) suggest an age of around ∼10 Ma for beginning of the shift to dominance of C_4 ecosystems. A reconsideration of the magnetostratigraphic constraints for the carbon isotopic records of pedogenic carbonate from the Siwaliks in Pakistan and India show that vegetation changed from a C_3 photosynthetic pathway to C_4 grasslands perhaps as early as 7.8 Ma and certainly by about 7.2 Ma. The shift in Nepal occurred somewhat later, starting after 7 Ma, and perhaps as late as 6 Ma. This ecological change was also recorded at about 7.2 Ma in leaf waxes recovered from the peninsular India at IODP Site U1457. Finally, magnetostratigraphic data from Argentina argue for a much later shift to C_4 dominance in South America and Australia in the Pliocene.

While it was previously hypothesized that a shift in vegetation on the Indian subcontinent could have been caused by uplift in the Himalayas through a change in local climate (enhanced Asian monsoon), Feakins et al. (This volume) show that there was no change in precipitation related isotopes through this interval. The connection to atmospheric CO_2 as a major driver is therefore of renewed interest for this regional transition, and some new pCO_2 reconstructions do indicate the possibility of a late Miocene drop, but more reconstructions are needed to secure such an interpretation. On land, rapid sediment accumulation rates in the Siwaliks in the Miocene could have led to enhanced carbon sequestration and the Siwaliks deposition ends abruptly soon after the C_4 transition in many sequences pointing to a change in basin dynamics. We wonder if the vegetation shift itself could be a feedback on the draw-down of atmospheric CO_2, perhaps via changing fluvial erosion on a grassy floodplain with enhanced erosion resulting in increased carbon burial (e.g., France-Lanord and Derry (1997); Derry and France-Lanord (1996)). In soils, the expansion of C_4 vegetation could have played a role in decreasing atmospheric CO_2 as C_4 grasslands can be more efficient at transferring CO_2 into soil than C_3 tropical forests. Understanding the terresrial and marine organic carbon feedbacks on the vegetation expansion look to be a promising direction for future enquiry.

NOTE TO REVIEWERS: THE REFERENCE LIST UNCAPITALIZES WORDS THAT SHOULD BE CAPITALIZED- THIS IS CAUSED BY A CHANGE IN THE AGU TEMPLATE - I HAVE NOTIFIED AGU OF THIS PROBLEM AND IT WILL BE FIXED PRIOR TO PUBLICATION.

References

Andrae, J., McInerney, F., Polissar, P., Sniderman, J., Howard, S., Hall, P., & Phelps, S. (2018). Initial expansion of c$_4$ vegetation in australia during the late pliocene. *Geophy. Res. Lett.*, *45*, 4831-4848. doi: 10.1029/2018GL077833

Appel, E., Rösler, W., & Corvinus, G. (1991). Magnetostragraphy of the miocene-pleistocene surai khola siwaliks in west nepal. *Geophys. J. Int.*, *105*, 191-198.

Backman, J., Raffi, I., Rio, D., Fornaciari, E., & Pälike, H. (2012). Biozonation and biochronology of miocene through pleistocene calcareous nanno-fossils from low and middle latitudes. *Newsl. Stratigr.*, *45*, 221-244. doi: 10.1127/0078-0421/2012/0022

Beerling, D., & Royer, D. (2011). Convergent cenozoic co$_2$ history. *Nature Geoscience*, *4*, 418-420. doi: 10.1038/ngeo1186

Behrensmeyer, A. K., Quade, J., Cerling, T. E., Kappelman, J., Khan, I., Copeland, P., . . . Latorre, C. (2007). The structure and rate of late miocene expansion of c4 plants: Evidence from lateral variation in stable isotopes in paleosols of the siwalik group, northern pakistan. *Geol. Soc. Am. Bull*, *119*, 1486-1505. doi: 10.1130/B26064.1

Bender, M., & Keigwin, L. D. (1979). Speculations about the upper miocene change in abyssal pacific dissolved bicarbonate δ^{13}c. *Earth Planet. Sci. Letters*, *45*, 383-393.

Berggren, W. A., Kent, D. V., Flynn, J. J., & Couvering, J. A. V. (1985). Cenozoic geochronology. *Geol. Soc. Amer. Bull.*, *96*, 1407–1418.

Billups, K. (2002). Late miocene through early pliocene deep water circulation and climate change viewed from the sub-antarctic south atlantic. *Paleogeo. Paleoclim. and Paleoecol.*, *185*, 287-307. doi: 10.1016/S0031-0182(02)00340-1

Brozovic, N., & Burbank, D. W. (2000). Dynamic fluvial systems and gravel progradation in the himalayan foreland. *Geol. Soc. Am. Bull.*, *112*, 394-412. doi: 10.1130/0016-7606(2000)112⟨394:dfsagp⟩2.0.co;2

Butler, R. F., Marshall, L. G., Drake, R. E., & Curtis, G. H. (1984). Magnetic polarity stratigraphy and 40K-40ar dating of late miocene and early pliocene continental deposits, catamarca province, NW argentina. *J. Geol.*, *92*, 623–636.

Cerling, T. E. (1992). Use of carbon isotopes in paleosols as an indicator of the p(co2) of the paleoatmosphere. *Global Biogeochem. Cycles*, *6*, 307-314. doi: 10.1029/92GB01102

Cerling, T. E., Harris, J., Macfadden, B. J., Leakey, M., Quade, J., Eisenmann, V., & Ehleringer, J. (1997). Global vegetation change through the miocene/pliocene boundary. *Nature*, *389*, 153-158. doi: 10.1038/38229

Cerling, T. E., Wang, Y., & Quade, J. (1993). Expansion of c4 ecosystems as an indicator of global ecological change in the late miocene. *Nature*, *361*, 344-345. doi: 10.1038/361344a0

Chen, S., Smith, S., Sheldon, N., & Strömberg, C. (2015). Regional-scale variability in the spread of grassland in the late miocene. *Paleogeo. Paleoclim. and Paleoecol.*, *437*, 42-52. doi: 10.1016/j.palaeo.2015.07.020

Chirouze, F., Dupont-Nivet, G., Huyghe, P., van der Beek, P., Chakraborti, T., Bernet, M., & Erens, V. (2012). Magnetostratigraphy of the neogene siwalik group in the far eastern himalaya: Kameng section, arunachal pradesh, india. *J. Asian Earth Sci.*, *44*, 117-135.

Cramer, B., Toggweiler, J. R., Wright, J. D., Katz, M., & Miller, K. G. (2009).

Ocean overturning since the late cretaceous: Inferences from a new benthic foraminiferal isotope compilation. *Paleocanography*, *24*, PA4216. doi: 10.1029/2008PA001683

Curry, W., & Miller, K. G. (1989). Oxygen and carbon isotope variation in pliocene benthic foraminifers of the equatorial atlantic. *Proceedings of the Ocean Drilling Program, Scientific Results*, *108*, 157-166. doi: 10.2973/odp.proc.sr.108.134.1989

Dahl, K., Oppo, D. W., Eglinton, T., Hughen, K., Curry, W., & Sirocko, F. (2005). Terrigenous plant wax inputs to the arabian sea: Implications for the reconstruction of winds associated with the indian monsoon. *Geochim. Cosmo. Acta*, *69*, 2547-2558. doi: 10.1016/j.gca.2005.01.001

Derry, L., & France-Lanord, C. (1996). Neogene growth of the sedimentary organic carbon reservoir. *Paleoceanography*, *11*, 267-275. doi: 10.1029/95pa03839

Diester-Haass, L., Billups, K., & Emeis, K. (2006). Late miocene carbon isotope records and marine biological productivity: Was there a (dusty) link. *Paleocanography*, *21*, PA4216. doi: 10.1029/2006PA001267

Dong, J., Liu, Z., An, Z., Liu, W., Zhou, W., & Qiang, X. (2018). Mid-miocene c_4 expansion on the chinese loess plateau under an enhanced asian summer monsoon. *J. Asian Earth Sci.*, *158*, 153-159. doi: 10.1016/j.jseaes.2018.02.014

Edwards, E., Osborne, C., Strömberg, C., Smith, S., & Consortium, C. G. (2010). The origins of c_4 grasslands: Integrating evolutionary and ecosystem science. *Science*, *328*, 587-591. doi: 10.1126/science.1177216

Feakins, S., Levin, N., Liddy, H., Sieracki, A., Eglinton, T., & Bonnefille, R. (2013). Northeast african vegetation change over 12 m.y. *Geology*, *41*, 295-298. doi: 10.1130/G33845.1

Feakins, S., Liddy, H., Tauxe, L., Galy, V., Feng, X., Tierney, J., . . . Warny, S. (This volume). Late miocene c4 expansion and hydrological change in the indus river catchment. *Paleoceanography and Paleoclimate*, in press. doi: 10.1029/2020PA00385

Fisher, R. L., Bunce, E., & et al. (1974). *Initial reports of the deep sea drilling project* (Vol. 24). U.S. Government Printing Office. doi: 10.2973/dsdp.proc.24.1974

Fornara, D., & Tilman, D. (2008). Plant functional composition influences rates of soil carbon and nitrogen accumulation. *J. Ecology*, *96*, 314-322. doi: 10.1111/j.1365-2745.2007.01345.x

Foster, G., Royer, D., & Lunt, D. (2017). Future climate forcing potentially without precedent in the last 420 million years. *Nature Communications*, *8*, 14845. doi: 10.1038/ncomms14845

Fox, D., & Koch, P. (2003). Tertiary history of c_4 biomass in the great plains, usa. *Geology*, *31*, 809-812. doi: 10.1130/g19580.1

France-Lanord, C., & Derry, L. (1997). Organic carbon burial forcing of the carbon cycle from himalayan erosion. *Nature*, *390*, 65-67. doi: 10.1038/36324

Ghosh, S., Sanyal, P., & Kumar, R. (2017). Evolution of c_4 plants and controlling factors: Insight from n-alkane isotopic values of nw indian siwalik paleosols. *Organic Geochem.*, *110*, 110-121. doi: 10.1016/j.orggeochem.2017.04.009

Gradstein, F., Ogg, J., Schmitz, M., & Ogg, G. (2012). *Geologic time scale 2012*. Amsterdam: Elsevier. doi: 10.1016/B978-0-444-59425-9.00005-6

Haq, B. U., Worsley, T. R., Burkle, L., Douglas, R. G., Keigwin, L. D., Opdyke, N., . . . Woodruff, F. (1980). Late miocene marine carbon-isotopic shift and synchroneity of some phytoplanktonic biostratigraphic events. *Geology*, *8*, 427-431. doi: 10.1130/0091-7613(1980)8⟨427:LMMCSA⟩2.0.CO;2

Harrison, T., Copeland, P., Hall, S., Quade, J., Burner, S., Ohja, T., & Kidd, W. (1993). Isotopic preservation of himalayan/tibetan uplift, denudation, climatic histories of two molasse deposits. *J. Geology*, *101*, 157-175. doi: 10.1086/648214

Harrison, T., & Yin, A. (2004, 01). Timing and processes of himalayan and tibetan uplift. *Himalayan Journal of Sciences*, *2*. doi: 10.3126/hjs.v2i4.847

Higgins, S., & Scheiter, S. (2012). Atmospheric co2 forces abrupt vegetation shifts locally, but not globally. *Nature*, *488*, 209-212. doi: 10.1038/nature11238

Hodell, D., Charles, C., Curtis, J., Mortyn, P., Ninnemann, U., & Venz, K. (2002). Data report: Oxygen isotope stratigraphy of odp leg 177 sites 1088, 1089, 1090, 1093, and 1094. In R. Gersonde, D. A. Hodell, & P. Blum (Eds.), (Vol. 177). Ocean Drilling Program. doi: 10.2973/odp.proc.sr.177.120.2003

Holbourn, A., Kuhnt, W., Clemens, S., Kochhann, K., Jöhnck, J., Lübbers, J., & Andersen, N. (2018). Late miocene climate cooling and intensification of southeast asian winter monsson. *Nature Communications*, *9*, 1-11. doi: 10.1038/s41467-018-03950-1

Johnson, N., Opdyke, N., Johnson, G., Lindsay, E., & Tahirkheli, R. A. K. (1982). Magnetic polarity stratigraphy and ages of siwalik group rocks of the potwar plateau, pakistan. *Paleogeo. Paleoclim. and Paleoecol.*, *37*, 17-42. doi: 10.1016/0031-0182(82)90056-6

Johnson, N., Stix, J., Tauxe, L., Cerveny, P. F., & Tahirkheli, R. A. K. (1985). Paleomagnetic chronology, fluvial processes and tectonic implications of the siwalik deposits near chinji. *Jour. Geology*, *93*, 27–40.

Keigwin, L. D. (1979). Late cenozoic stable isotope stratigraphy and paleoceanography of dsdp sites from the east equatorial and central north pacific ocean. *Earth and Plan. Sci. Lett*, *45*, 361-382. doi: 10.1016/0012-821X(79)90137-7

Keigwin, L. D., & Corliss, B. H. (1986). Stable isotopes in late middle eocene to oligocene forminifera. *Geol. Soc. Amer. Bull.*, *97*, 335–345. doi: 10.1130/0016-7606(1986)97⟨335:SIILME⟩2.0.CO;2

Kleinert, K., & Strecker, M. (2001). Climate change in response to orographic barrier uplift: Paleosol and stable isotope evidence from the late neogene santa maría basin, northwestern argentina. *G.S.A. Bulletin*, *113*, 728-742. doi: 10.1130/0016-7606(2001)113⟨0728:CCIRTO⟩2.0.CO;2

LaBrecque, J. L., Kent, D. V., & Cande, S. C. (1977). Revised magnetic polarity time scale for late cretaceous and cenozoic time. *Geology*, *5*, 330–335.

Latorre, C., Quade, J., & McIntosh, W. (1997). The expansion of c$_4$ grasses and global change in the late miocene: Stable isotope evidence from the americas. *Earth and Planet. Sci. Lett..*, *146*, 83-96.

Meigs, A., Burbank, D. W., & Beck, R. (1995). Middle-late miocene (¿10 ma) formation of the main boundary thrust in the western himalaya. *Geology*, *23*, 423-426. doi: 10.1130/0091-7613(1995)023⟨0423:MLMMFO⟩2.3.CO;2

Mejia, L., Méndez-Vicente, A., Abrevaya, L., Lawrence, K., Ladlow, C., Bolton, C., ... Stoll, H. (2017). A diatom record of co2 decline since the miocene. *Earth and Planet. Sci. Lett.*, *479*, 18-33. doi: 10.1016/j.epsl.2017.08.034

Molnar, P., England, P., & Martinod, J. (1993). Mantle dynamics, uplift of the tibetan plateau and the indian monsoon. *Rev. Geophys.*, *31*, 357-396. doi: 10.1029/93RG02030

Morgan, M., Kingston, J., & Marino, B. (1994). Carbon isotopic evidence for the emergence of c4 plants in the neogene from pakistan and kenya. *Nature*, *367*, 162-165.

Neupane, P., Gani, M., Gani, N., & Huang, Y. (2019). Neogene vegetation shift in the nepalese siwalik, himalayas: A compound-specific isotopic study of lipid biomarkers. *The Depositional Record*, *00*, 1-11. doi: 10.1002/dep2.91

Ojha, T., Butler, R. F., DeCelles, P., & Quade, J. (2009). Magnetic polarity stratigraphy of the neogene foreland basin deposits of nepal. *Basin Research*, *21*, 61-90. doi: 10.1111/j.1365-2117.2008.00374.x

Opdyke, N. D., Lindsay, E., Johnson, G. D., Johnson, N. M., Tahirkheli, R. A. K., & Mirza, M. A. (1979). Magnetic polarity stratigraphy and vertebrate paleontology of the upper siwalik subgroup of northern pakistan. *Palaeogeogr.*

Palaeoclimat. Palaeoecol., *27*, 1-34. doi: 10.1016/0031-0182(79)90091-9

Osborne, C. (2008). Atmosphere, ecology and evolution: what drove the miocene expansion of c$_4$ grasslands? *J. Ecol.*, *96*(35-45). doi: 10.1111/j.1365-2745.2007.01323.x

Pagani, M., Freeman, K., & Arthur, M. A. (1999). Late miocene atmospheric co$_2$ concentrations and the expansion of c$_4$ grasses. *Science*, *285*, 876-879. doi: 10.1126/science.285.5429.876

Pandey, D., Clift, P., Kulhanek, D., & Scientists, E. . (2016). Site u1457. *Proc. IODP*, *355*. doi: 10.14379/iodp.proc.355.104.2016

Party, T. S. (1974). Site 235. *Initial Reports of the DSDP*, *24*. doi: 10.2973/dsdp.proc.24.106.1974

Polissar, P., Rose, C., Uno, K., Phelps, S., & deMenocal, P. (2019). Synchronous rise of african c$_4$ ecosystems 10 million years ago in the absence of aridification. *Nature Geoscience*, *12*, 657-660. doi: 10.1038/s41561-019-0399-2

Quade, J. (2014). The carbon, oxygen, and clumped isotopic composition of soil carbonate in archeology. In (Vol. 14, p. 129-143). Elsevier. doi: 10.1016/B978-0-08-095975-7.01211-0

Quade, J., Cater, J., T.P., O., Adam, J., & Harrison, T. (1995). Late miocene environmental change in nepal and the northern indian subcontinent: Stable isotopic evidence from paleosols. *Geol. Soc. Am. Bull*, *107*, 1381-1397. doi: 10.1130/0016-7606(1995)107⟨1381:LMECIN⟩2.3.CO;2

Quade, J., & Cerling, T. E. (1995). Expansion of c4 grasses in the late miocene of northern pakistan: evidence from stable isotopes in paleosols. *Paleogeo. Paleoclim. and Paleoecol.*, *115*, 91-116. doi: 10.1016/0031-0182(94)00108-k

Quade, J., Cerling, T. E., & Bowman, J. R. (1989). Development of asian monsoon revealed by marked ecological shift during the latest miocene in northern pakistan. *Nature*, *342*, 163-166.

Raffi, I., Backman, J., Fornaciari, E., Pälike, H., Rio, D., Lourens, L., & Hilgen, F. (2006). A review of calcareous nannofossil astrobiochronology encompassing the past 25 million years. *Quat. Sci. Rev.*, *25*, 3113-3137. doi: 10.1016/j.quascirev.2006.07.007

Rao, A. (1993). Magnetic-polarity stratigraphy of upper siwalik of north-western himalayan foothills. *Current Research, PtB, Geol. Surv. Canada*, *64*, 863-873.

Raymo, M. E., & Ruddiman, W. F. (1992). Tectonic forcing of late cenozoic climate. *Nature*, *359*(6391), 117–122. Retrieved from https://doi.org/10.1038/359117a0 doi: 10.1038/359117a0

Retallack, G. (2007). Cenozoic paleoclimate on land in north america. *J. Geology*, *115*, 271-294. doi: 10.1086/512753

Retallack, G. (2013). Global cooling by grassland soils of the geologic past and near future. *Annu. Rev. Earth Planet. Sci.*, *41*, 69-86. doi: 10.1146/annurev-earth-050212-124001

Retallack, G., Bajpai, S., Liu, X., Kapur, V., & Pandey, S. (2018). Advent of strong south asian monsoon by 20 million years ago. *The Journal of Geology*, *126*, 1-24. doi: 10.1086/694766

Rösler, W., Metzler, W., & Appel, E. (1997). Neogene magnetic polarity stratigraphy of some fluviatile siwalik sections, nepal. *Geophys. J. Int.*, *130*, 89-111. doi: 10.1111/j.1365-246x.1997.tb00990.x

Routledge, C., Kulhanek, D., Tauxe, L., Scardia, G., Singh, A., Steinke, S., . . . Saraswat, R. (2019). A revised chronostratigraphic framework for international ocean discovery program expedition 355 sites in laxmi basin, eastern arabian sea. *Geological Magazine*, *in press*. doi: 10.1017/S0016756819000104

Ruddiman, W., Sarnthein, M., Baldauf, J., & Party, S. S. (n.d.). Site 659. *Proc. ODP., Init. Rept.*, *108*, 221-325.

Sangode, S., Kumar, R., & Ghosh, S. (1996). Magnetic polarity stratigraphy of the siwalik sequence of haripur area (h.p.), nw himalaya. *J. Geol. Soc. India*, *47*,

788   683-704. doi: http://www.geosocindia.org/index.php/jgsi/article/view/68308

789 Sanyal, P., Bhattacharya, S., Kumar, R., Ghosh, S., & Sangode, S.   (2004).   Mio-
790   pliocene monsoonal record from himalayan foreland basin (indian siwalik) and
791   its relation to vegetational change.   *Paleogeo. Paleoclim. and Paleoecol.*, *205*,
792   23-41.

793 Schneider, D. (1995). Paleomagnetism of some leg 138 sediments: detailing miocene
794   magnetostratigraphy. *Proc. ODP, Sci. Results.*, *138*, 59-72.

795 Ségalen, L., Lee-Thorp, J., & Cerling, T. E.   (2007).   Timing of c_4 grass expansion
796   across sub-saharan africa. *J. Human Evol.*, *53*, 549-559.

797 Shackleton, N., Hall, M., & Boersma, A.   (1984).   Oxygen and carbon isotope data
798   from leg 74 foraminifers. *Init. Reports, DSDP*, *74*, 599-612. doi: 10.2973/dsdp
799   .proc.74.115.1984

800 Singh, S., Parkash, B., Awasthi, A., & Kumar, S.   (2011).   Late miocene record of
801   palaeovegation from siwalik paleosols of the ramnagar sub-basin, india.   *Cur-*
802   *rent Science*, *100*, 213-222.

803 Sosdian, S., Greenop, R., Hain, M., Foster, G., Pearson, P., & Lear, C.   (2018).
804   Constraining the evolution of neogene ocean carbonate chemistry using the
805   boron isotope ph proxy.   *Earth and Planet. Sci. Lett.*, *498*, 362-376.   doi:
806   10.1016/j.epsl.2018.06.017

807 Spiesman, B., Kummel, H., & Jackson, R.   (2018).   Carbon storage poten-
808   tial increases with increasing ratio of c_4 to c_3 grass cover and soil pro-
809   ductivity in restored tallgrass prairies.   *Oecologia*, *186*, 565-576.   doi:
810   10.1007/s00442-017-4036-8

811 Tauxe, L., Monaghan, M., Drake, R., Curtis, G., & Staudigel, H. (1985). Paleomag-
812   netism of miocene east african rift sediments and the calibration of the grts. *J.*
813   *Geophys. Res.*, *90*, 4639-4646.

814 Tauxe, L., & Opdyke, N. D.   (1982).   A time framework based on magnetostratig-
815   raphy for the siwalik sediments of the khaur area, northern pakistan.   *Palaeo-*
816   *geogr. Palaeoclimat. Palaeoecol.*, *37*, 43-61.

817 Theyer, F., & Hammond, S. R.   (1974).   Cenozoic magnetic time scale in deep-sea
818   cores; completion of the neogene. *Geology*, *October 1974*, 487-492.

819 Tipple, B., & Pagani, M.   (2007).   The early origins of terrestrial c_4 photosynthesis.
820   *Ann. Rev. Earth and Planet. Sci.*, *35*, 435-461.   doi: 10.1146/annurev.earth.35
821   .031306.140150

822 Tipple, B., & Pagani, M.   (2010).   A 35 myr north american leaf-wax compound-
823   specific carbon and hydrogen isotope record: Implications for c_4 grasslands and
824   hydrologic cycle dynamics.   *Earth and Planet. Sci. Lett.*, *299*, 250-262.   doi:
825   10.1016/j.epsl.2010.09.006

826 Tremblay, M., Fox, M., Schmidt, J., Tripathy-Lang, A., Wielicki, M., Harrison, T., &
827   Zeitler, D., P. andShuster. (2015). Erosion in southern tibet shut down at ∼10
828   ma due to enhanced rock uplift within the himalaya.   *Proc. Nat. Acad. Sci.*,
829   *112*, 12030-12035. doi: 10.1073/pnas.1515652112

830 Tripati, A., Roberts, C., & Eagle, R. (2009). Coupling of co_2 and ice sheet stability
831   over major climate transitions of the last 20 million years.   *Science*, *326*, 1394-
832   1397. doi: 10.1126/science.1178296

833 Uno, K., Cerling, T. E., Harris, J., Kunimatsu, Y., Leakey, M., Nakatsukasa, M.,
834   & H., N.   (2011).   Late miocene to pliocene carbon isotope record of differen-
835   tial diet change among east african herbivores.   *Proc. Nat. Acad. Sci.*, *108*,
836   6509-6514. doi: 10.1073/pnas.1018435108

837 Uno, K., Polissar, P., Jackson, K., & deMenocal, P. B.   (2016).   Neogene biomarker
838   record of vegetation change in eastern africa. *Proc. Nat. Acad. Sci.*, *113*, 6355-
839   6363. doi: 10.1073/pnas.1521267113

840 Van der Burgh, J., Visscher, H., Dilcher, D., & Kürschner, W.   (2009).   Paleoatmo-
841   spheric signatures in neogene fossil leaves.   *Science*, *260*, 1788-1790.   doi: 0
842   .1126/science.260.5115.1788

Vincent, E., Killingley, J. S., & Berger, W. (1980). The magnetic epoch-6 carbon shift: a change in the ocean's $^{13}|c/^{12}c$ ratio 6.2 million years ago. *Marine Micropaleont.*, *5*, 185-203.

Vögeli, N., Najman, Y., van der Beek, P., Huyghe, P., Wynn, P., Govin, G., ... Sachse, D. (2017). Lateral variations in vegetation in the himalaya since the miocene and implications for climate evolution. *Earth and Planet. Sci. Lett.*, *471*, 1-9. doi: 10.1016/j.epsl.2017.04.037

Woodruff, F., & Savin, S. (1989). Miocene deepwater oceanography. *Paleocanography*, *4*, 87-140. doi: 10.1029/PA004i001p00087

Woodruff, F., Savin, S. M., & Douglas, R. G. (1981). Miocene stable isotope record: a detailed deep pacific ocean study and i its paleoclimatic implications. *Science*, *212*, 665-668. doi: 10.1016/0377-8398(81)90031-1

Wright, J. D., Miller, K. G., & Fairbanks, R. G. (1992). Early and middle miocene stable isotopes: Implications for deepwater circulation and climate. *Paleoceanography*, *7*, 357-389. doi: 10.1029/92PA00760

Yang, Y., Tilman, D., Furey, G., & Lehman, C. (2019). Soil carbon sequestration accelerated by resotration of grassland biodiversity. *Nature Communications*, *10*, 718. doi: 10.1038/s41467-019-08636-w

Zhou, H., Helliker, B., Huber, M., Dicks, A., & Akcay, E. (2018). C_4 photosynthesis and climate through the lens of optimality. *Proc. Nat. Acad. Sci.*, *115*, 12057-12062. doi: 10.1073/pnas.1718988115

5 Supplemental Information
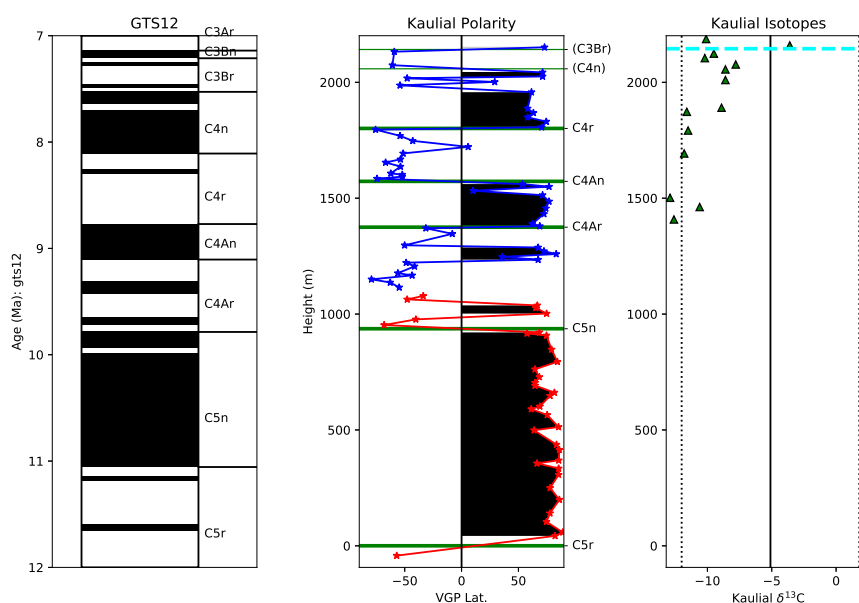
Figure S1

Details for sections in Figure 6. See Table 1 for data sources. left: Magnetic polarity time scale of Gradstein et al. (2012). middle: Virtual Geomagnetic Pole (VGP) positions for sites in the Kaulial Kas Section plotted against stratigraphic height. Those in parentheses were added or modified in this paper; those without are as in the original publication. Solid green lines are the Chron boundaries as identified to the right. c) Carbon isotopes from paleosol carbonate nodules. Dotted lines are C_3 and C_4 end-

873   members for soil carbonates. C_3-C_4 transition boundary (boundaries) as dashed cyan
874   horizontal line(s).

875   Figure S2
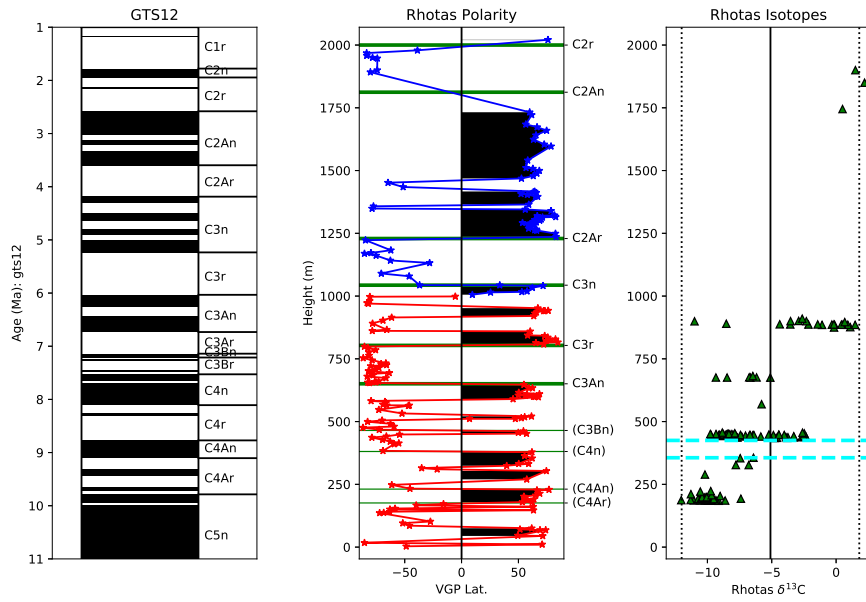
876

877   Same as Figure S1 but for the Rhotas Section.

878   Figure S3
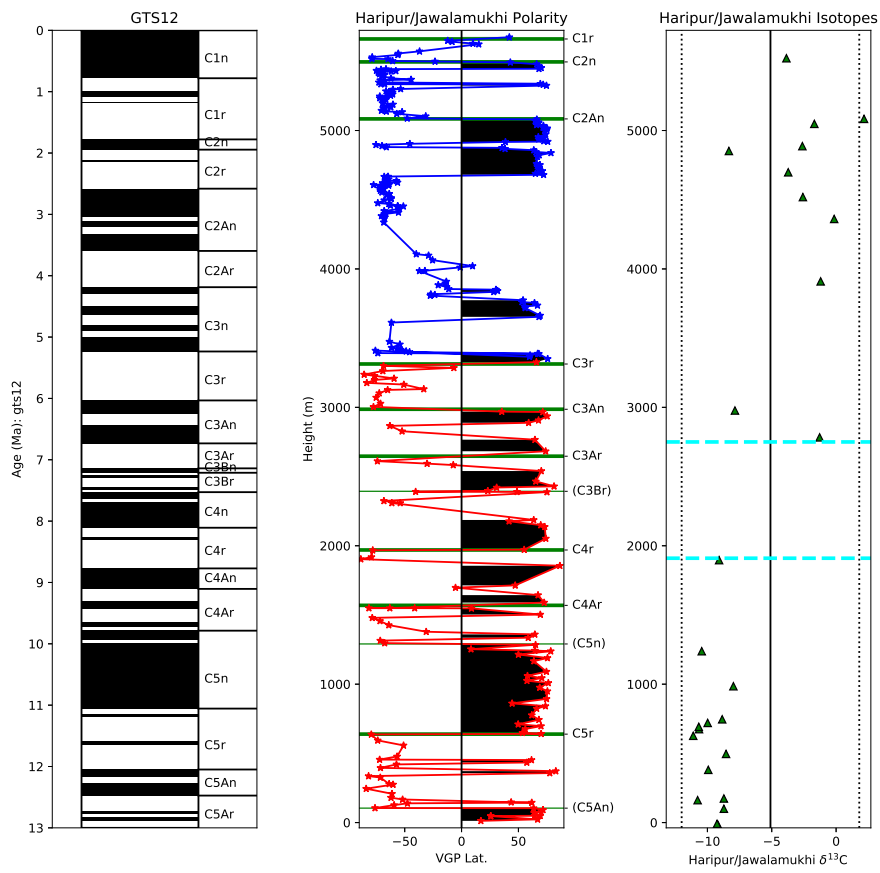
879

880   Same as Figure S1 but for the Jawalamukhi/Haripur Sections.

881   Figure S4
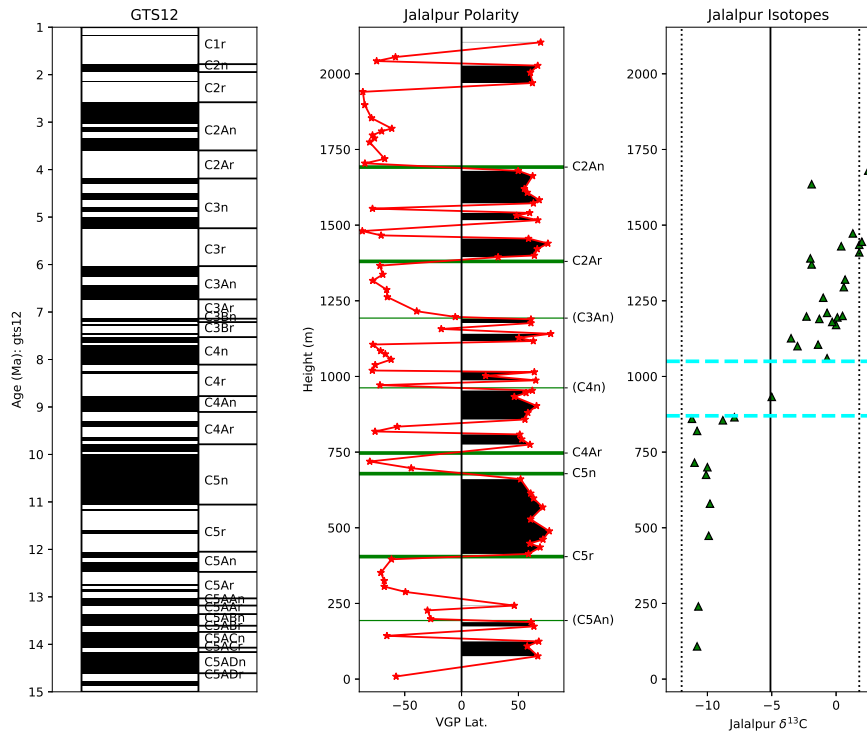
882

883   Same as Figure S1 but for the Jalalpur Section.

884 Figure S5
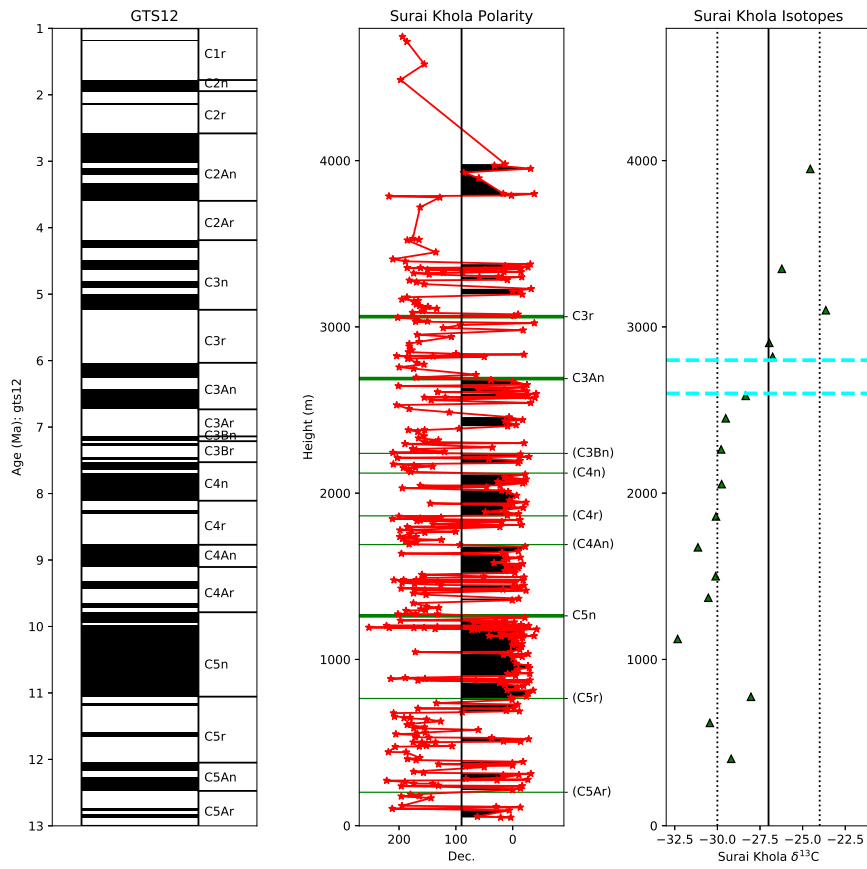
885

886 Same as Figure S1 but for the Surai Khola Section. Middle panel is declination (not
887 VGP). Isotopic data are C_{27} *n*-alkane data. Dotted lines are the limits of C_3, C_4 for plant
888 waxes.

⁸⁸⁹ Figure S6
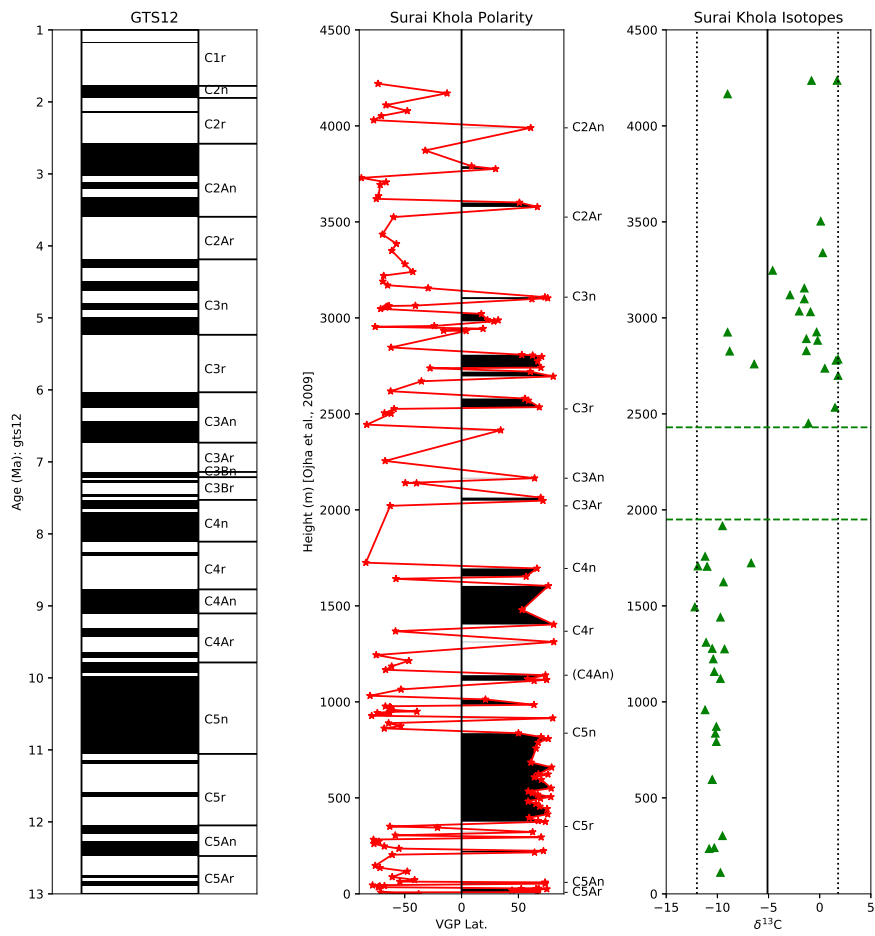
⁸⁹⁰

⁸⁹¹ Same as Figure S1 but for the alternate Surai Khola Section of Ojha et al. (2009)
⁸⁹² and Quade et al. (1995). Middle panel is declination (not VGP).

893   Figure S7
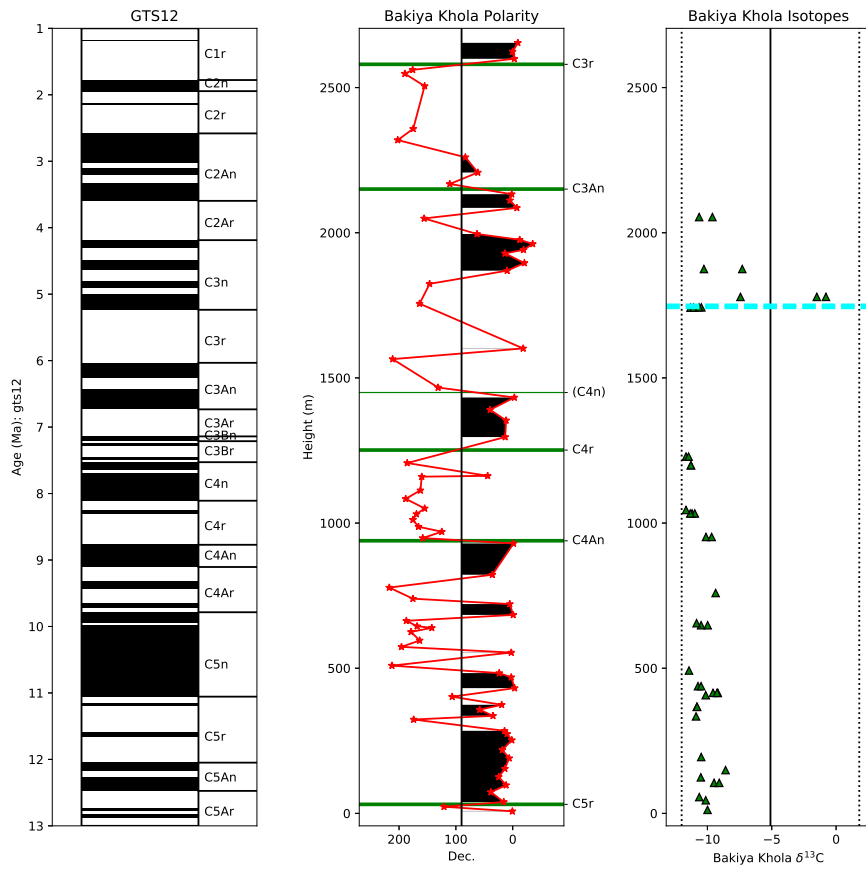
894

895   Same as Figure S1 but for the Bakiya Khola Section. Middle panel is declination
896   (not VGP).

897   Figure S8
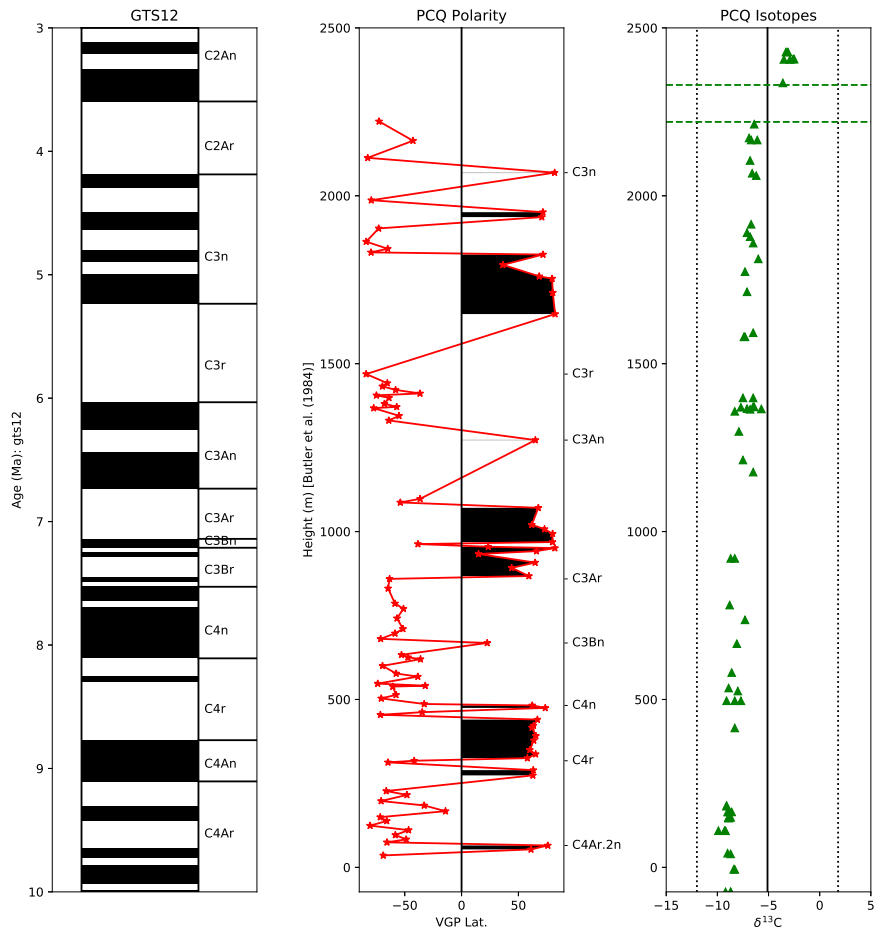
898

899   Same as Figure S1 but for the Puerta de Corral Quermado (PCQ) Section.

Figure 1.

a) 600 ppm

| C3 + forest | C3 dominant | C3>C4 | C3=C4 | C4>C3 | C4 dominant |
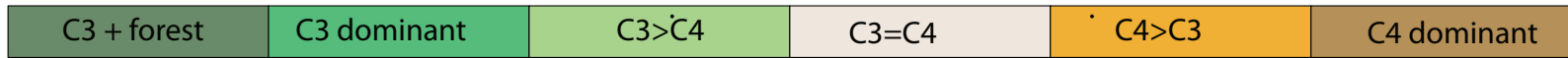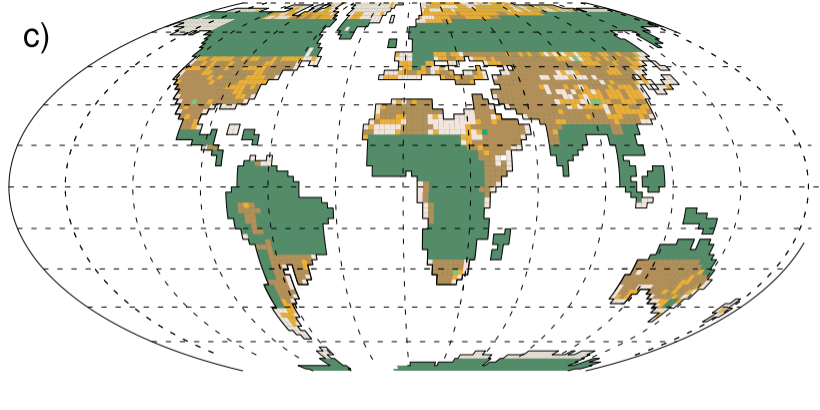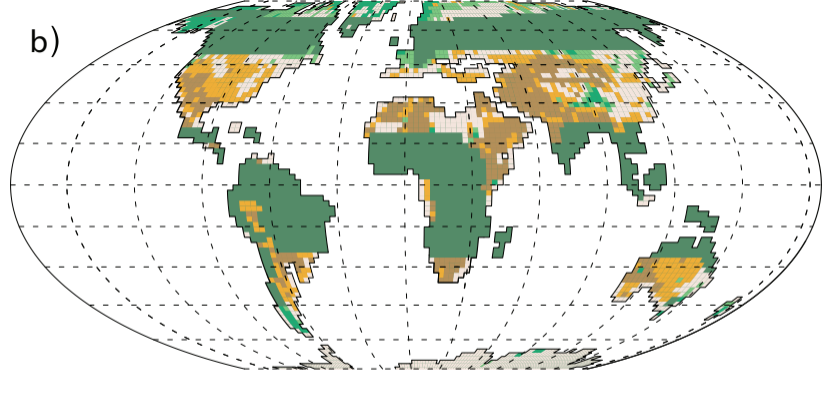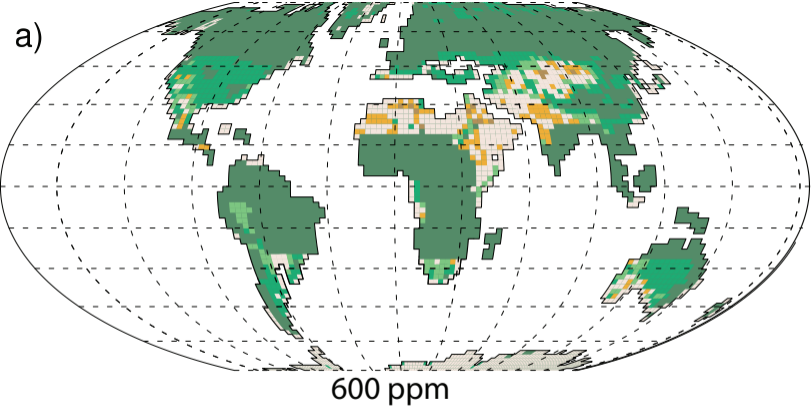
Figure 2.

Figure 3.

Figure 4.

a)

DSDP552
DSDP207   DSDP310
                                      ODP 659
DSDP235   ODP1146
                                      ODP0667
Fig. 1b   DSDP158   ODP 959
DSDP231   DSDP238   ODP0846
           DSDP214   DSDP077 DSDP289
DSDP525   PCQ   DSDP357
DSDP360   DSDP527   DSDP208
ODP1088

b)

Kaulial Kas
Jalalpur   Rhotas
Jawalamukhi
Haripur-Kolar
Surai Khola
Bakiya Khola

U1457

Figure 5.

DSDP310 (NP)
DSDP207 (NP)
ODP0667 (NA)
DSDP552 (NA)
DSDP525 (SA)
DSDP527 (SA)
DSDP357 (SA)
ODP1088 (IN)
DSDP360 (IN)
DSDP238 (IN)
DSDP214 (IN)
DSDP158 (EP)
DSDP077 (EP)
DSDP289 (EP)
ODP0846 (EP)
DSDP208 (SP)

positive <= δ^{13}C (normalized) => negative

Depth in sediment below Amaurolithus FO (m)

−60   −40   −20   0   20

Figure 6.

a) GTS12
b) KK δ¹³C
c) R δ¹³C
d) JH δ¹³C
e) JP δ¹³C
f) SK δ¹³C
g) BK δ¹³C

Figure 7.

Figure 8.

Figure 9.

a)

Depth (mcd)

Grain size

Clay | Silt | Sand | Gravel

b)

- ◀ PF
- ▶ CN
- ▲ Pmag

Unit 5

Unit 4

Unit 3

Mass-Transport Deposit

Unit 2

U3

U2

U1

Age (Ma) - Routledge et al. (2019)

c)

- ◀ PF
- ▶ CN
- ▲ Pmag

Unit 5

Unit 4c

Unit 4b

Unit 4a

Unit 3

Mass-Transport Deposit

Unit 2

Age (Ma) (this paper)

Lithology

- Carbonate ooze/stone
- Clay/Claystone
- Silt/Siltstone
- Sand/Sandstone
- Calcarenite
- Carbonate breccia

Figure 10.

a) GTS12

C1r
C2n
C2r
C2An
C2Ar
C3n
C3r
C3An
C3Ar
C3Bn
C3Br
C4n
C4r
C4An
C4Ar
C5n
C5r
C5An
C5Ar

Age (Ma): gts12

b) U1457 Polarity

(C3Ar)
B N. amplificus
(C3Br.2r)
B Amaurolithus spp.
(C3Br.2n)
(C4n.1r)

Composite Depth (cmd)

Inclination

c) U1457 Isotopes

U1457 δ^{13}C

Figure 11.

a) ODP 659   b) ODP 959   c) DSDP 235   d) DSDP 231

Depth (mcd/mbsf)

$\delta^{13}C$ (C35 n-alkane) $\delta^{13}C$ (C$_{35}n-$alkane) $\delta^{13}C$ (C$_{35}n-$-alkane) $\delta^{13}C$ (C$_{30}n$-alkanoic acids)
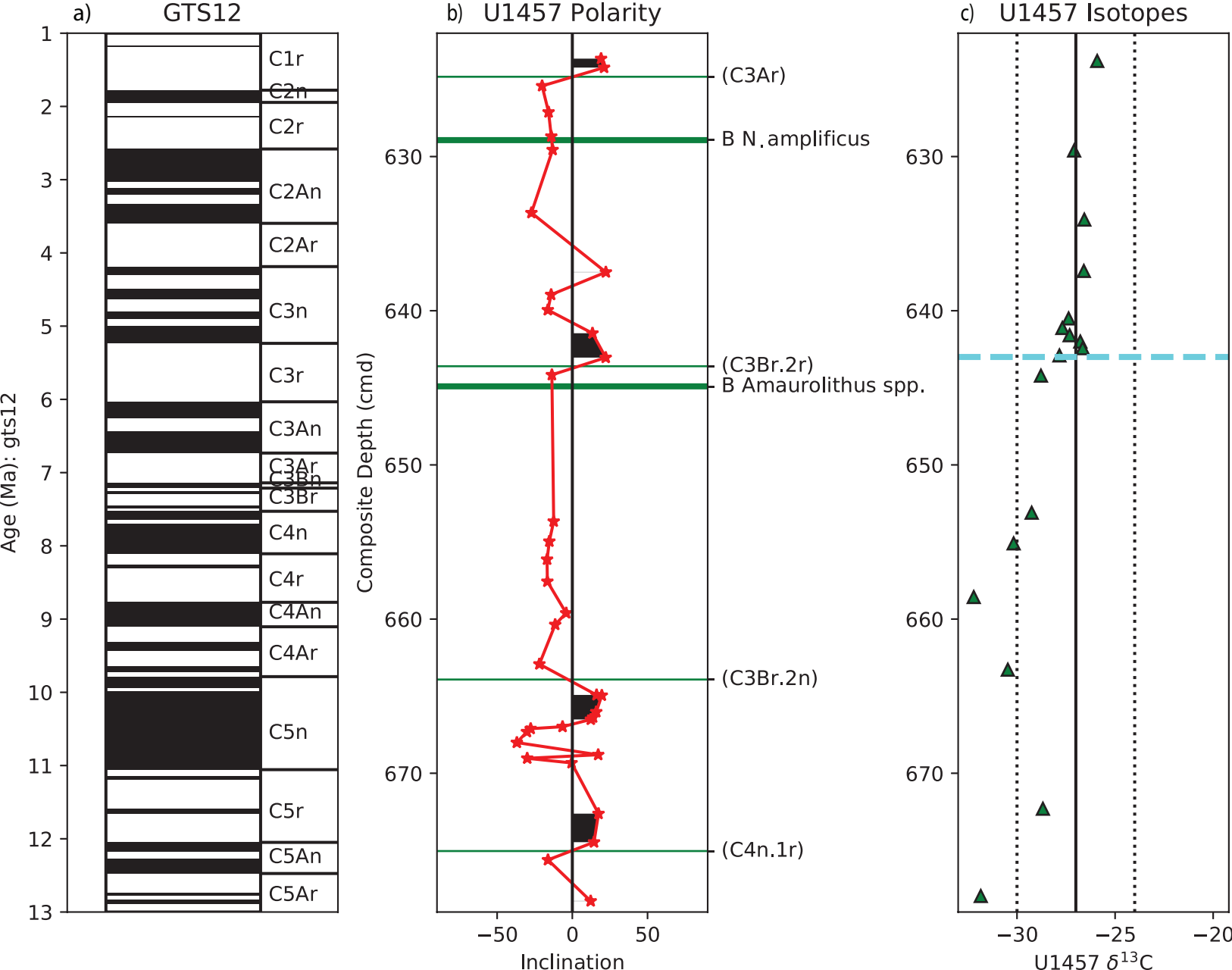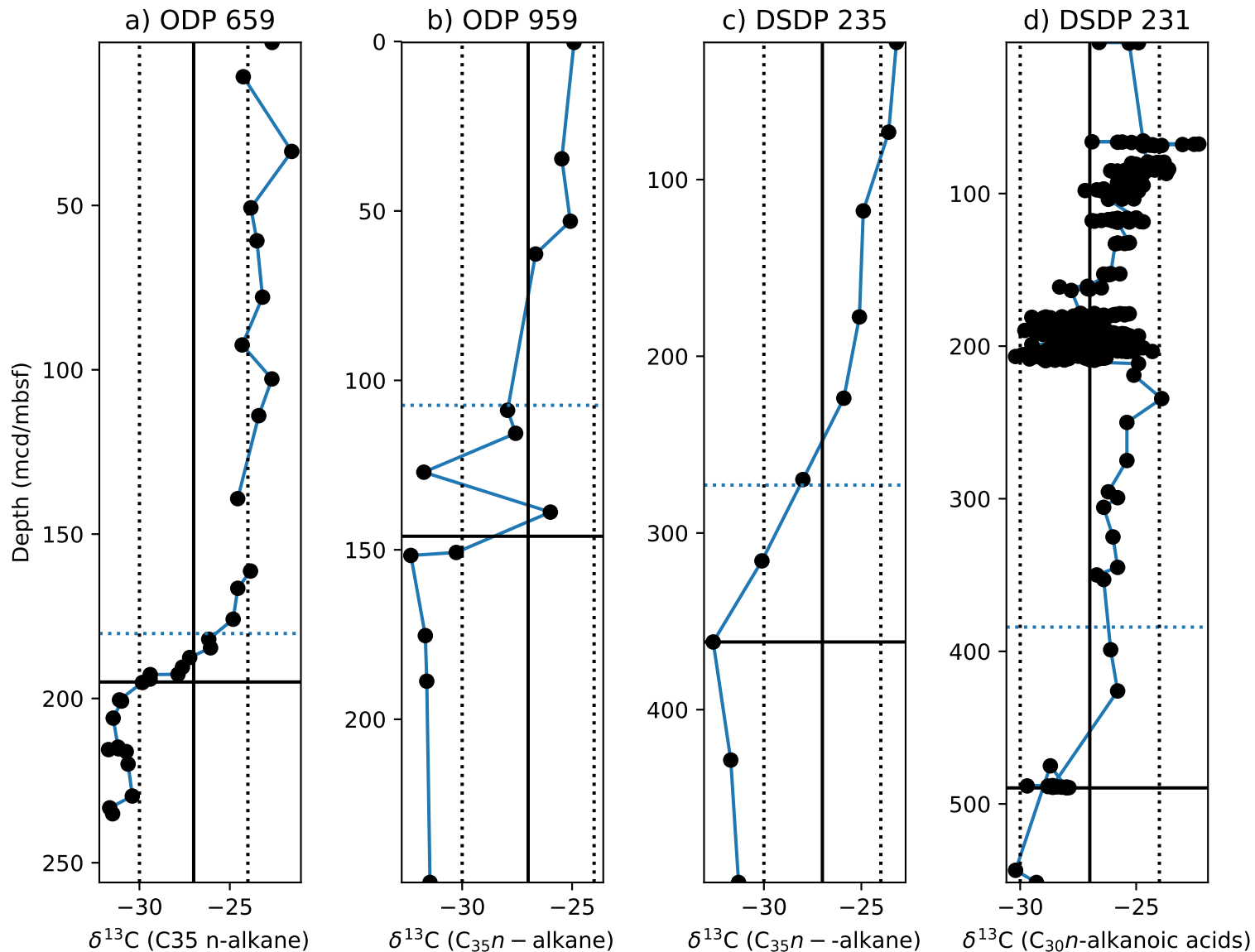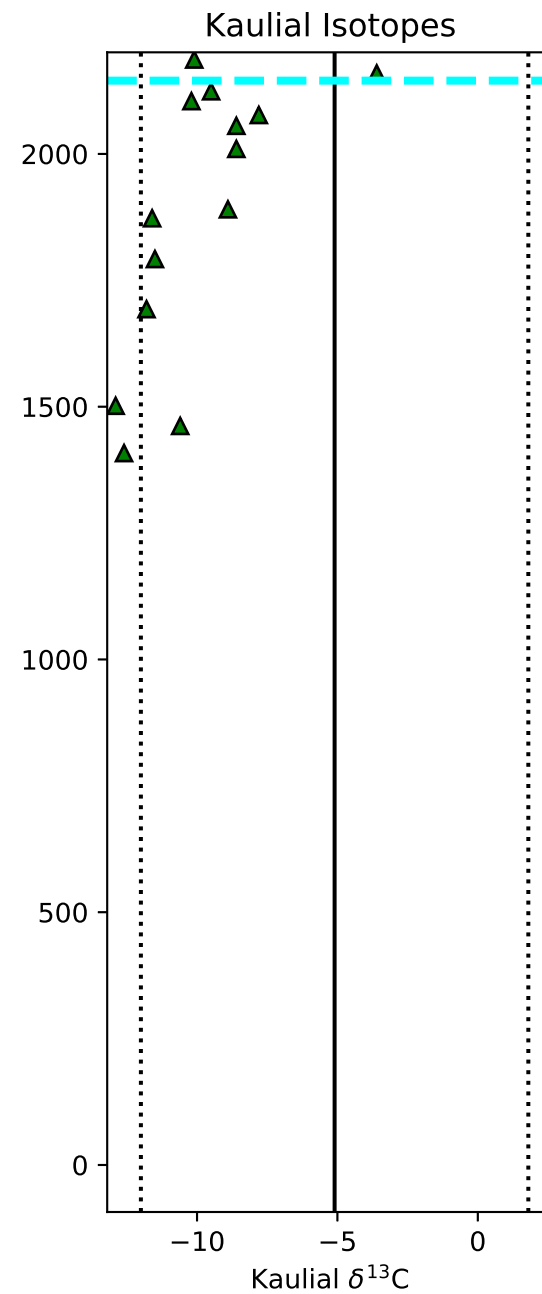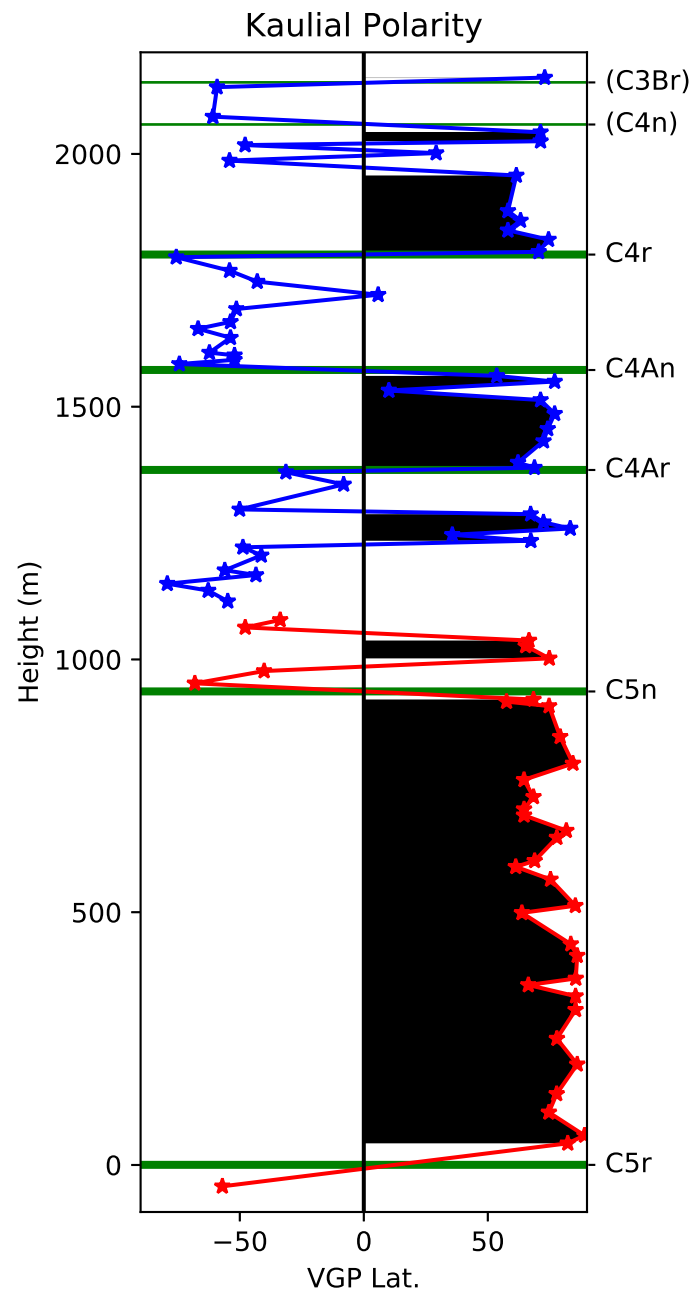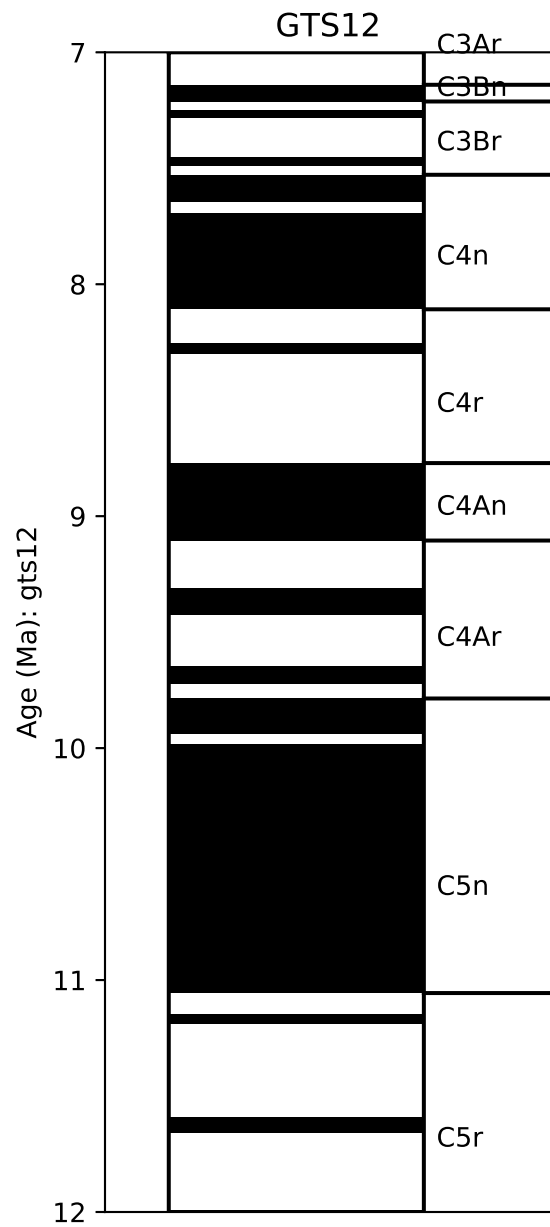
Figure S1.

Figure S2.

Figure S3.

Figure S4.

GTS12

Jalalpur Polarity

Jalalpur Isotopes

Age (Ma): gts12

C1r	
C2n	
C2r	
C2An	
C2Ar	
C3n	
C3r	
C3An	
C3Ar	
C3Bn	
C3Br	
C4n	
C4r	
C4An	
C4Ar	
C5n	
C5r	
C5An	
C5Ar	
C5AAn	
C5AAr	
C5ABn	
C5ABr	
C5ACn	
C5ACr	
C5ADn	
C5ADr	

Height (m)

VGP Lat.

C2An
C2Ar
(C3An)
(C4n)
C4Ar
C5n
C5r
(C5An)

Jalalpur δ^{13}C

Figure S5.

Figure S6.

Figure S7.